W. May

Potential future changes in the Indian summer monsoon due to greenhouse warming: analysis of mechanisms in a global time-slice experiment

Abstract In this study the potential impact of the anticipated increase in the greenhouse gas concentrations on different aspects of the Indian summer monsoon is investigated, focusing on the role of the mechanisms leading to these changes. Both changes in the mean aspects of the Indian summer monsoon and changes in its interannual variability are considered. This is done on the basis of a global time-slice experiment being performed with the ECHAM4 AGCM at a high horizontal resolution of T106. The experiment consists of two 30-year simulations, one representing the present-day climate (period: 1970–1999) and one representing the future climate (period: 2060–2089). The time-slice experiment predicts an intensification of the mean rainfall associated with the Indian summer monsoon due to the general warming, while the future changes in the large-scale flow indicate a weakening of the monsoon circulation in the upper troposphere and only little change in the lower troposphere. The intensification of the monsoon rainfall in the Indian region is related to an intensification of the atmospheric moisture transport into this region. The weakening of the monsoon flow is caused by a pronounced warming of the sea surface temperatures in the central and eastern tropical Pacific and the associated alterations of the Walker circulation. A future increase of the temperature difference between the Indian Ocean and central India as well as a future reduction of the Eurasian snow cover in spring would, by themselves, lead to a strengthening of the monsoon flow in the future. These two mechanisms compensate for the weakening of the low-level monsoon flow induced by the warming of the tropical Pacific. The time-slice experiment also predicts a future increase of the interannual variability of both the rainfall associated with the Indian summer monsoon and of the large-scale flow. A major part of this increase is accounted for by enhanced interannual variability of the sea surface temperatures in the central and eastern tropical Pacific.

W. May (✉)
Danish Meteorological Institute,
Lyngbyvej 100, 2100 Copenhagen, Denmark
E-mail: may@dmi.dk

1 Introduction

During the boreal summer season, the climate in Southeast Asia in general and in India in particular is dominated, respectively, by the Asian and Indian summer monsoon. The Asian summer monsoon returns with remarkable regularity every year and provides the rainfall for crops that sustain over 60% of the earth's population. The monsoon circulation is mainly driven by the differential heating of the Indian Ocean and the adjacent land areas (e.g. Krishnamurti and Ramanathan 1982). Therefore, it is in part related to the Eurasian snow cover, as indicated in observational studies (e.g. Hahn and Shukla 1976; Dickson 1984; Sankar-Rao et al. 1996). Sensitivity experiments with atmospheric general circulation models (AGCMs) have shown that when spatially coherent excessive snow cover is imposed in Eurasia in spring, the monsoon circulation is relatively weak in the following summer (e.g. Douville and Royer 1996; Ferranti and Molteni 1999). There may also exist an inverse relationship between the Asian summer monsoon and the El Niño/Southern Oscillation (ENSO) phenomenon (e.g. Rasmusson and Carpenter 1983; Webster and Yang 1992). These observational studies have found that drought years over Southeast Asia (weak monsoon) are often related to warm sea surface temperature (SST) anomalies in the central and eastern tropical Pacific (El Niño) and wet years (strong monsoon) to anomalously cold SST anomalies (La Niña). These relationships have also been identified in modelling studies (e.g. Ju and Slingo 1995; Lau and Nath 2000). However, the strength of the Indian summer

monsoon is also affected by the SSTs in the Indian Ocean. Joseph et al. (1994) reported, for instance, on a delay of the monsoon onset, generally indicating reduced precipitation during the monsoon season, in relation to warm SST anomalies at and south of the equator during the pre-monsoon season (March through May). In their modelling study Chandrasekar and Kitoh (1998) actually found a significant response over the entire Indian region to idealized SST anomalies placed in the Indian Ocean just south of the equator, namely a decrease in the monsoon precipitation and a weakening of the monsoon circulation. In a series of GCM experiments, Meehl and Arblaster (2002) investigated the effect of anomalous SST-patterns in the tropical Indian Ocean and in the tropical Pacific and of anomalous land surface temperatures in Asia during the pre-monsoon season on the Indian summer monsoon. They found that each of these anomalous conditions can effect the strength of the summer monsoon by themselves. But the anomalous SSTs in the tropical ocean basins lead to a larger response of the monsoon compared to the anomalous meridional temperature gradient over Asia. Further, the location of the SST anomalies in the tropical Indian Ocean is important, with warm SST anomalies throughout the tropical Indian Ocean producing enhanced rainfall over the ocean and South Asian land areas, and warm SST anomalies near the equatorial Indian Ocean producing increased rainfall locally with decreased rainfall over the South Asian land areas.

Due to its enormous socio-economic impact in the region, the possible impact of the anticipated increase in the greenhouse gas concentrations on the Indian summer monsoon has become an important issue, which has been addressed in several modelling studies employing coupled GCMs. Meehl and Washington (1993) obtained, for instance, an increase in the summer monsoon precipitation in a climate with doubled CO_2, related to the stronger surface warming over the Asian continent than over the Indian Ocean. Bhaskaran et al. (1995) and, similarly, Hu et al. (2000) found a northward shift and intensification of the monsoon rainfall, which they attributed to the increased difference between land and ocean temperatures. Kitoh et al. (1997) noted an apparent paradox between the circulation and precipitation changes simulated by MRI's coupled climate model. Despite a weakening of the low-level monsoon winds over the Arabian Sea, summer monsoon rainfall over India increases due to a larger moisture content in the warmer troposphere. May (2002) also found an intensification of the rainfall in the Indian region during the monsoon season in response to the general warming, while the future changes in the large-scale flow indicate a weakening of the monsoon circulation. The increase in the regional rainfall is caused by an intensification of the moisture transport into the Indian region. According to Meehl and Arblaster (2003), the predicted intensification of the monsoon rainfall associated with the greenhouse warming is related to increased moisture source from the warmer Indian Ocean. Douville et al. (2000) compared

the impact of a doubling of CO_2 on the Asian summer monsoon as simulated by four different coupled GCMs. All models reveal a stronger warming over the Asian continent than over the Indian Ocean but a significant spread of the changes in summer precipitation. These changes are accompanied by a general weakening of the monsoon circulation, indicating that the response of the monsoon rainfall is not solely related to the changes in the large-scale dynamics. Observations actually indicate a weakening of the large-scale aspects of the Indian summer monsoon (Stephenson et al. 2001), while the all-India rainfall reveals only little evidence of a change in recent historical observations (Rupa Kumar et al. 1992).

According to some recent studies (Hu et al. 2000; Lal et al. 2000; Meehl and Arblaster 2003), the increase in the mean monsoon rainfall is accompanied by an increase in the interannual variability. While Hu et al. (2000) related the increase in the interannual variability to a corresponding increase of the SST variability in the tropical Pacific Ocean, Meehl and Arblaster (2003) assigned it primarily to warmer mean SSTs in the tropical Pacific Ocean, accompanied by enhanced evaporation variability. In the latest assessment report of the Intergovernmental Panel on Climate Change (IPCC; Houghton et al. 2001) the results regarding the Asian summer monsoon have been summarized as follows: the warming associated with increasing greenhouse gas concentrations will "likely" cause an increase of the Asian summer monsoon precipitation variability. The changes in the mean duration and the strength of the monsoon depend on the details of the emission scenarios. The confidence in such projections is also limited by how well the climate models simulate the detailed seasonal evolution of the monsoons.

Obviously, coupled climate models with a typical resolution of 300–500 km cannot explicitly capture the fine-scale structures that characterize climate variables such as near-surface temperature and precipitation in many parts of the globe and, therefore, may have difficulties in properly simulating the regional distributions of these variables. This is in particular the case, when the orographic forcing, such as for the monsoon rainfall in India with the Western Ghats and the Himalayas plays an important role. One way to improve the simulation of the regional phenomena, is to increase the horizontal resolution of the GCM considerably, to about 100 km, so that smaller spatial and temporal scales are explicitly resolved (e.g. Bengtsson et al. 1995; Stratton 1999; May 2001). As for the simulation of the Asian summer monsoon, Martin (1999) found that in the case of the HadAM2B AGCM the high horizontal resolution provided extra detail in the precipitation distribution, but the mean monsoon simulation was hardly altered and the systematic errors remain. Apparently, the systematic errors in the monsoon simulation by HadAM2B are not a result of the coarse resolution, but may be related to problems with the physical parametrizations of the model. On the other hand, for the ECHAM3 and

ECHAM4 AGCMs, Dümenil and Bauer (1998) observed a better simulation of the tropical easterly jet over South Asia, the Indian Ocean and Africa at the high horizontal resolution. Further, the simulation of several aspects of the Indian summer monsoon, such as the distribution of precipitation in the vicinity of the Western Ghats, the strength and position of the monsoon trough across northeast India, and the strength of the low-level winds over the Bay of Bengal with ECHAM4 benefited considerably from the high horizontal resolution (Stendel and Roeckner 1998). Stephenson et al. (1998) found in their study of the impact of the horizontal resolution (ranging from 200 to 600 km) on the simulation of the Asian summer monsoon by ARPEGE-CLIMAT both an improvement and a reduction of the quality of the simulation when the resolution was increased, because some of the model's systematic errors became accentuated at higher resolution.

In this study the potential impact of the anticipated increase in the greenhouse gas concentrations on different aspects of the Indian summer monsoon is investigated. Furthermore, the role of the mechanisms leading to these changes is addressed. This is done on the basis of a time-slice experiment, which has been performed with the ECHAM4 AGCM at a high horizontal resolution of T106 (May and Roeckner 2001, hereafter referred to as "MR01"). The time-slice experiment consists of two 30-year simulations, one representing the present-day climate (period: 1970–1999) and one representing the future climate (period: 2060–2089). The study is an extension of May (2002) in several aspects: (a) additional features of the Indian summer monsoon area considered, (b) the role of the different mechanisms leading to the predicted changes in the Indian summer monsoon is discussed in detail, and (c) the interannual variability of the Indian summer monsoon is included. According to May (2003) (hereafter referred to as "M03"), the high-resolution version of ECHAM4 simulates both the seasonal mean characteristics and the sub-seasonal variability of the Indian summer monsoon very realistically, making the changes predicted in this particular experiment very plausible. MR01 investigated the impact of the model resolution on the annual mean climate change. They found, among others, stronger overall changes in the hydrological cycle for the high horizontal resolution, with a particularly strong increase in precipitation over the equatorial oceans. Further, differences in the precipitation response were found especially in areas with strong topographical control. Therefore, also the simulation of the Indian summer monsoon and of its future changes probably depends on the model resolution, and the influence of the model resolution on the Indian summer monsoon will be considered in this study.

The work is organized as follows: in Sect. 2 the time-slice experiment is introduced. Subsequently, the results regarding the large-scale circulation (Sect. 3) and regarding the hydrological cycle (Sect. 4) and the underlying mechanisms are described. In Sect. 5 the interannual variability is considered, and a summary and the conclusions (Sect. 6) complete the study.

2 Time-slice experiment

The study is based on a time-slice experiment (also referred to as "TSL") with the ECHAM4 AGCM at a high horizontal resolution of T106 with 160×320 grid points on the corresponding Gaussian grid and 19 vertical levels. (Roeckner et al. 1996a; Stendel and Roeckner 1998). Two simulations, each covering a period of 30 years, have been performed, one representing the present-day climate (TSL1; 1979–1999) and one representing the future climate after an effective doubling of the CO_2 concentration in the atmosphere (TSL-2; 2060–2089). During these two time-slices the lower boundary forcing, i.e. monthly mean values of the SSTs and of the sea-ice extent and sea-ice thickness, have been prescribed as obtained from a climate change simulation with the ECHAM4/OPYC coupled atmosphere–ocean GCM at a low horizontal resolution of T42, corresponding to 64×128 grid points, and 19 vertical levels as well (Roeckner et al. 1999). Moreover, the temporal evolution of the atmospheric concentrations of the important greenhouse gases has been prescribed in the same way as in the respective climate change simulation: according to observations until 1990 and after 1990 according to IPCC scenario IS92a (Houghton et al. 1992). Changes in the aerosol concentrations have not been considered in these experiments. Further details on the greenhouse gas forcing in these simulations can be found in (Roeckner et al. 1999) or MR01. Similar to the time-slice experiment, the two periods of the greenhouse gas experiment with the low-resolution coupled model, 1970–1999 and 2060–2089, are referred to as "GHG-1" and "GHG-2", respectively. In the further course of this study, also the ECMWF re-analyses for the period 1979–1993 (e.g. Gibson et al. 1997; referred to as "ERA") are considered.

In ECHAM4/OPYC flux corrections in the annual means of heat and freshwater are applied (Bacher et al. 1998) in order to avoid long-term drifts of the annual mean SSTs. Nevertheless, the seasonal evolution of the SSTs, such as in the tropical Pacific, is also very realistically simulated. Further, this model is able to catch many features of the observed interannual SST variability in the tropical Pacific (Roeckner et al. 1996b). This includes amplitude, lifetime and frequency of occurrence of El Niño events and also the phase locking of the SST anomalies to the annual cycle. Also the simulated atmospheric response to the pronounced variations of the SSTs in the tropical Pacific is in accord with observations. As for the Indian Ocean, the coupled model gives slightly (≈ 1 °C) too warm SSTs during summer southwest of the Indian peninsula, in the Bay of Bengal and west of Indonesia, while in spring the simulated SSTs in the entire Indian Ocean are very close to observations (Bacher et al. 1998).

A thorough discussion of the changes in the mean global climate inferred from the two time-slices is given in MR01. In M03, on the other hand, the quality of the simulation of the Indian summer monsoon in TSL-1 is investigated, considering aspects of the seasonal mean monsoon as well as of its sub-seasonal variability. According to this, the various aspects of the Indian summer monsoon are simulated very realistically in the time-slice representing the present-day climate, though some deficiencies remain. These are a warm bias of the mean temperature over land, leading to a too strong temperature gradient between the Indian Ocean and the land areas to the north, an underestimation of precipitation near the west coast of the Indian peninsula, and a too weak upper level monsoon flow. The underestimation of precipitation near the west coast affects the pattern describing the day-to-day variability of rainfall during the monsoon season, since the strength of the centre of action located in this area is considerably underestimated in the time-slice experiment. In particular, TSL-1 is superior to another AMIP-type simulation with the high-resolution version of ECHAM4, where observed monthly mean values of the SSTs and of the sea-ice extent have been prescribed as lower boundary forcing.

Horizontal wind
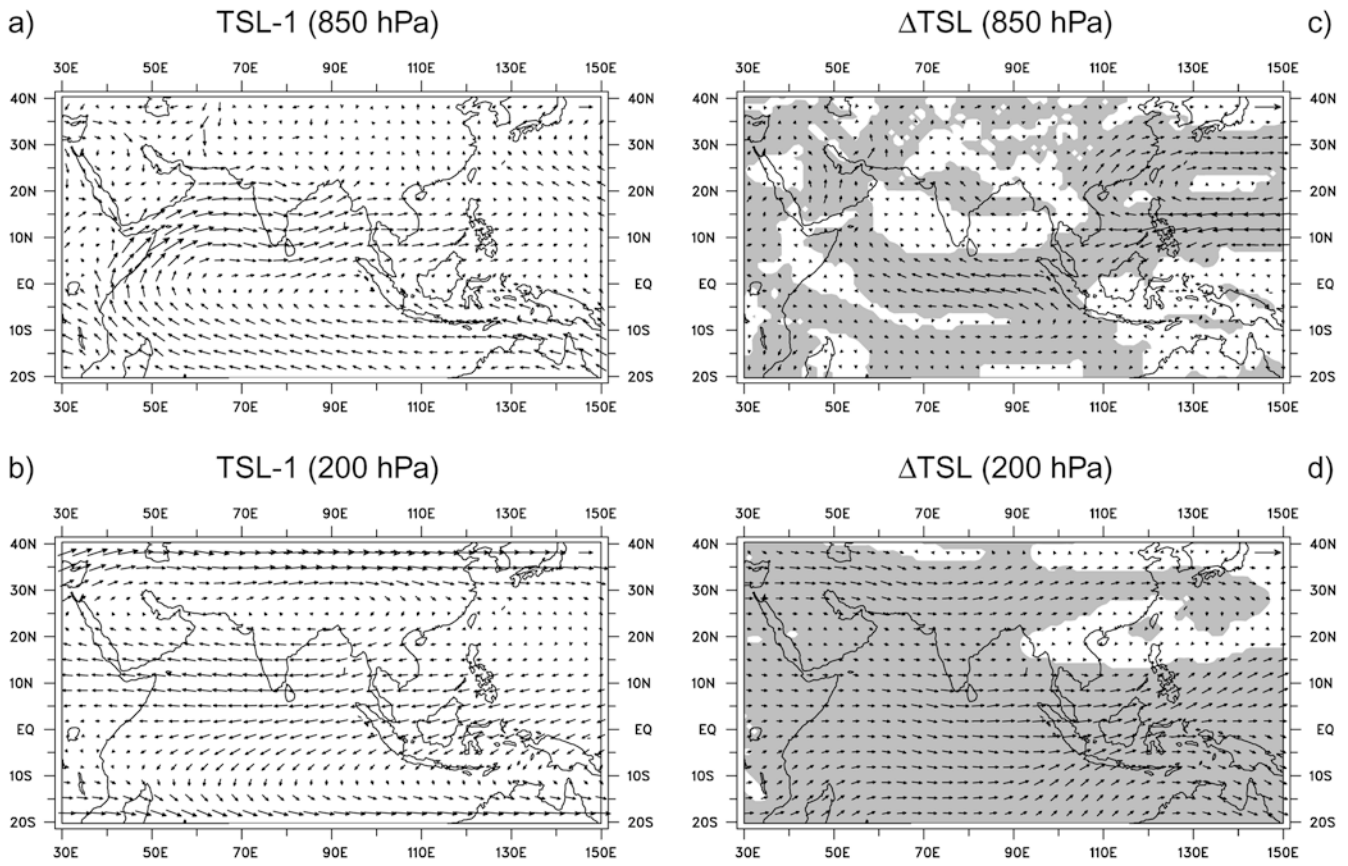
Fig. 1 Seasonal mean (June, July, August and September; "JJAS") horizontal wind for TSL-1 at **a** 850 hPa and **b** 200 hPa. Further, the difference between TSL-2 and TSL-1 ("ΔTSL") at **c** 850 hPa and **d** 200 hPa. The *shading* indicates the significance of the differences at the 95% level. Units are m/s. The *arrows* in the *upper right corner* represent 4 m/s (**c**), 8 m/s (**a, d**), and 16 m/s (**b**), respectively
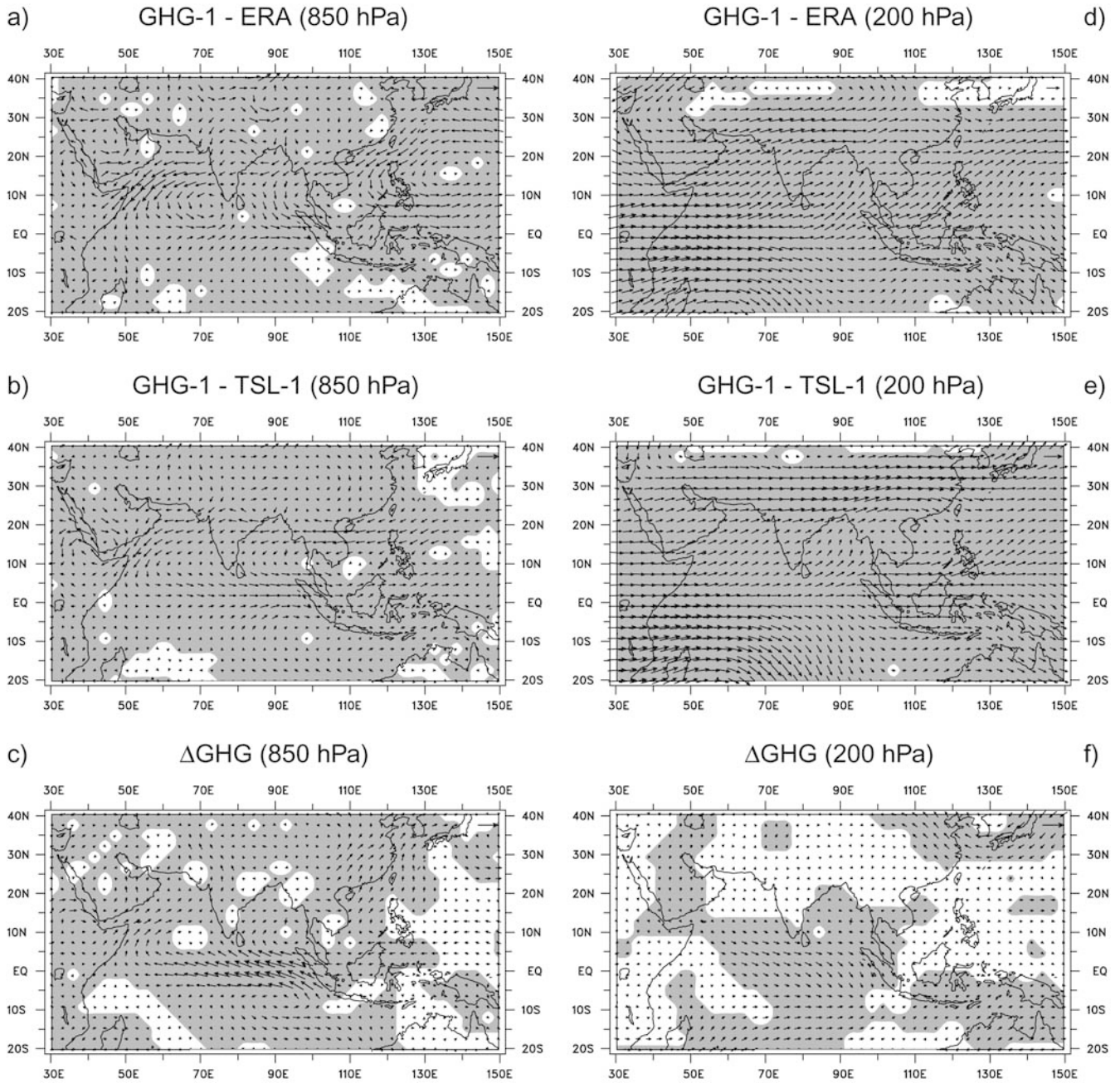
3 Large-scale circulation

3.1 Monsoon flow

During the established phase of the Indian summer monsoon (June to September), the large-scale flow in the lower troposphere (at 850 hPa) as simulated in TSL-1 is characterized by a cross-equatorial flow near the African coast, forming the "Somali-jet," and a westerly flow over the Arabian Sea and the Indian subcontinent, extending further into the eastern parts of Southeast Asia (Fig. 1a). Over the Bay of Bengal, TSL-1 reveals the characteristic cyclonic flow pattern with a southerly flow from the Bay of Bengal into Bangladesh and northeast India in association with the monsoon trough. In the upper troposphere (at 200 hPa), the simulated large-scale flow during the monsoon season is dominated by a northward shift of the subtropical westerly jet and a band of easterly winds over the northern and tropical Indian Ocean, also referred to as the "tropical easterly jet" (Fig. 2b). An extended anticyclone is located over the southern part of the Arabian Peninsula, Pakistan, northern India, and the northeastern part of Southeast Asia. As a consequence of the westerly winds in the lower troposphere and the easterly winds in the upper troposphere, there is a positive vertical wind shear in the tropics and the Northern Hemisphere subtropics centred over the Indian Ocean. In the lower troposphere, the most pronounced deviation from observations is a slight underestimation of the westerly winds over the Arabian Sea, while in the upper troposphere the model markedly underestimates the easterly winds over the northern and tropical Indian Ocean (M03). As a consequence, the simulated vertical wind shear is considerably too small in this region.

For the future, TSL predicts a deformation of the monsoon flow in the lower troposphere, in combination with a strengthening in some areas and a weakening in others (Fig. 1b). The Somali-jet, for instance, is stronger and extends further downstream over the Arabian Sea. Over the northern part of the Indian peninsula, the westerly winds are reduced, while over the southern part the westerly winds are virtually unchanged. At the same time, the northerly winds over the northeastern part of the Indian peninsula and the southerly winds over the Bay of Bengal are reduced, indicating a weakening of the

Horizontal wind

a)
GHG-1 - ERA (850 hPa)

d)
GHG-1 - ERA (200 hPa)

b)
GHG-1 - TSL-1 (850 hPa)

e)
GHG-1 - TSL-1 (200 hPa)

c)
ΔGHG (850 hPa)

f)
ΔGHG (200 hPa)

Fig. 2 As Fig. 1, but for the differences **a** between GHG-1 and ERA, **b** between GHG-1 and TSL-1, and **c** between GHG-2 and GHG-1 ("ΔGHG") at 850 hPa (*left column*) and 200 hPa (*right column*). The *shading* indicates the significance of the differences at the 97.5 **a, b, d, e** and the 95% level **c, f**, respectively. Units are m/s. The *arrows* in the *upper right corner* represent 8 m/s, except for (**c**) with 4 m/s

monsoon trough in the future. Over the tropical Indian Ocean TSL predicts, on the other hand, a strengthening and a northward shift of the band with easterly winds. In the upper troposphere, TSL predicts a considerable reduction of the tropical easterly jet in the future, indicated by relatively strong westerly wind anomalies over southern India and the northern and tropical Indian Ocean (Fig. 1d). At the same time, the subtropical jet is shifted southward, in particular in the area around the Persian Gulf. By this, the strength of the monsoon flow in the upper troposphere is considerably reduced, also leading to a marked reduction of the easterly vertical wind shear in the Indian region. This is consistent with a number of coupled GCMs, which also predict a reduction of the upper-level monsoon flow in response to the increased level of CO_2(Douville et al. 2000). In

summary, TSL predicts a weakening of the monsoon flow in the Indian region as a consequence of the anticipated increase in the greenhouse gas concentrations, with the reduction being more pronounced in the upper troposphere.

Since at the high horizontal resolution small spatial and temporal scales are explicitly resolved and the orography is better represented, the simulation of the Indian summer monsoon is likely to be improved compared to a low-resolution GCM. In order to investigate whether this actually is case, the simulation of the monsoon flow in GHG, that is the simulation that has provided the lower-boundary forcing for TSL, is compared to TSL and ERA as well.

Although GHG-1 is also able to capture the general structure of the monsoon flow in the lower as well as in the upper troposphere, a number of marked deviations from the observations can be found. As for the lower troposphere, GHG-1 significantly underestimates the strength of the Somali jet and of the westerly flow over the Arabian Sea, the Indian peninsula, the Bay of Bengal and further into Southeast Asia (Fig. 2a). Also the intensity of the monsoon trough and, hence, of the cyclonic flow centred over Bangladesh is underestimated. The cross-equatorial flow, on the other hand, is overestimated in most of the Indian Ocean basin. Over the western subtropical Pacific, GHG-1 is characterized by marked cyclonic flow anomalies. Some of these deficiencies are also found for TSL-1, but the deviations from ERA are considerably smaller (M03). This can also be seen from Fig. 2b, where the differences between GHG-1 and TSL-1 are shown. The general structure of the anomalous flow is very similar to the differences between GHG-1 and ERA, indicating that the aforementioned deficiencies of GHG-1 are significantly reduced in TSL-1 or have even disappeared, such as the problems with the cross-equatorial flow or the monsoon trough. This tendency is also found in the upper troposphere, where the deviations from ERA (Fig. 2d) and from TSL-1 (Fig. 2e) also have very similar general structures. GHG-1 is, for instance, characterized by anomalous westerly winds over most of the Indian Ocean and Southeast Asia (Fig. 2d). In the area between the equator and about 20°N, this indicates a marked underestimation of the strength of the easterly tropical jet. Further to the north, the westerly wind anomalies are part of an anomalous cyclonic flow pattern that weakens and distorts the extended anticyclone ranging from the southern part of the Arabian peninsula to the northeastern part of Southeast Asia. Moreover, in the latitudinal band between 5°S and 20°N, the inflow from the western Pacific into the region over the Indian Ocean is suppressed in GHG-1. And over the western subtropical Pacific, an anomalous anticyclonic flow pattern in the upper troposphere accompanies the cyclonic flow anomalies in the lower troposphere (see Fig. 2a).

As compared to TSL (see Fig. 1c), GHG predicts a somewhat larger change of the low-level monsoon flow near the equator, both with regard to the cross-equatorial flow and the flow along the equator, and within the Somali jet (Fig. 2c). Further, GHG predicts a slightly stronger inflow into the region over the Bay of Bengal from the eastern part of the tropical Indian Ocean. Over the subtropical western Pacific, on the other hand, GHG does not show the anticyclonic flow anomalies predicted in TSL. This difference may be related to the low-resolution model's deficiency to properly simulate the large-scale flow in this region with an anomalous cyclonic flow pattern in GHG-1 (see Fig. 2b). In the upper troposphere, GHG predicts significantly weaker changes in the large-scale flow, with significant westerly wind anomalies (weaker, though) only occurring over the central part of the Indian Ocean (Fig. 2f). That is the weakening of the upper-level monsoon flow is considerably less pronounced in GHG. This difference between GHG and TSL is probably related to the general underestimation of the upper-level flow in the low-resolution model (see Fig. 2e). Further, the low-resolution model does not properly simulate the inflow from the western Pacific into the region over the Indian Ocean, thus suppressing the weakening (see later) influence of the warming in the tropical Pacific on the Indian summer monsoon.

3.2 Dynamical monsoon indices

According to Webster and Yang (1992), the vertical shear of the zonal wind component between 850 and 200 hPa in the area (Equator –20°N, 40–110°E) can be used as a dynamically based index to describe the strength of the Indian summer monsoon. Goswami et al. (1999), on the other hand, proposed the vertical shear of the meridional wind component in the area (10–30°N, 70–110°E) as another circulation index for the Indian summer monsoon, focusing on the local Hadley circulation. They found that the latter index is better correlated with the monsoon rainfall in the Indian region than the index proposed by Webster and Yang (1992).

Table 1 shows, among others, the estimates of these two indices for the two time-slices and the respective differences between TSL-2 and TSL-1. As a consequence of the prevailing westerly winds in the lower troposphere (see Fig. 1a) and the easterly winds in the upper troposphere (see Fig. 1b), the vertical shear of the zonal wind component ("U-shear") is positive, indicating an easterly vertical wind shear. The positive values of the vertical shear of the meridional wind component ("V-shear"), indicating a northerly vertical wind shear, are due to the fact that the northerly shear in the eastern part of the respective area exceeds the southerly wind shear (negative values of V-shear) in the western part. In the lower troposphere northerly winds prevail in the western part of the area and southerly winds in the eastern part in association with the cyclonic flow pattern (see Fig. 1a). In the upper troposphere, on the other hand, southerly winds occur on the western side of the anticyclone centred over Southeast Asia and southerly

Table 1 Indices for the Indian summer monsoon

	U-shear (m/s)	V-shear (m/s)	IR-rain (mm/d)	IB-rain (mm/d)
TSL-1	19.57	1.91	5.88	5.92
TSL-2	16.84	2.01	6.67	6.55
DIFF	−2.73**	0.10	0.78*	0.63*
REL DIFF	−13.94**	5.36	13.30*	10.72*
STD (TSL-1)	1.54	0.50	0.70	0.66
STD (TSL-2)	2.60	0.55	0.95	0.71
RATIO	2.86	1.20	1.83	1.17

See text for the definitions of the indices. In addition to the mean values for the two time-slices (TSL-1 and TSL2), the differences between TSL-2 and TSL-1 (DIFF), and the relative differences with regard to TSL-1 (REL DIFF; [%]) are given. ** and * indicate differences exceeding a 99.99% and a 99.9% level of significance, respectively. Further, the standard deviation of the interannual variations (STD (TSL-...) and the ratio of the variance of the interannual variations between TSL-2 and TSL-1 (RATIO; dimensionless)

winds on its eastern side (see Fig. 1b). The values are somewhat smaller than for observations, i.e. 23.13 m/s for U-shear and 2.87 m/s for V-shear according to the ERA. These deficiencies are mainly caused by the model's difficulties in simulating the monsoon flow in the upper troposphere (M03).

For the future, TSL predicts a significant reduction of U-shear (≈14%) for the reasons described in the previous section and a slight increase of V-shear (≈5%). The latter is due to the fact that the decrease of the southerly shear in the eastern part of the area exceeds the reduction of the northerly shear in the eastern part, to a large extent due to changes in the lower troposphere, characterized by a weakening of the cyclonic flow pattern over northeast India and the Bay of Bengal (see Fig. 1c).

3.3 Temperatures in the Indian region

Since the monsoon circulation is mainly driven by the differential heating of the Indian Ocean and the adjacent land areas (e.g. Krishnamurti and Ramanathan 1982), regional differences of the warming due to the anticipated increase in the greenhouse gas concentrations possibly affect the strength of the Indian summer monsoon. Figure 3, therefore, shows the near-surface temperatures in May, that is the month preceding the Indian summer monsoon.

TSL-1 simulates temperatures between 28 and 32 °C over the northern and equatorial Indian Ocean, with values above 30 °C occurring only to the south and west of the Indian peninsula (Fig. 3a). In most of India, on the other hand, temperatures exceed 36 °C, with temperatures close to 40 °C occurring in the semi-arid areas in northwest India. These regional temperature variations lead to a temperature difference of 8 to 10 °C between the Indian Ocean and central India just before the onset of the summer monsoon. TSL-1 is, however, characterized by somewhat too high temperatures over India as a consequence of problems with the parame-

Near-surface temperature
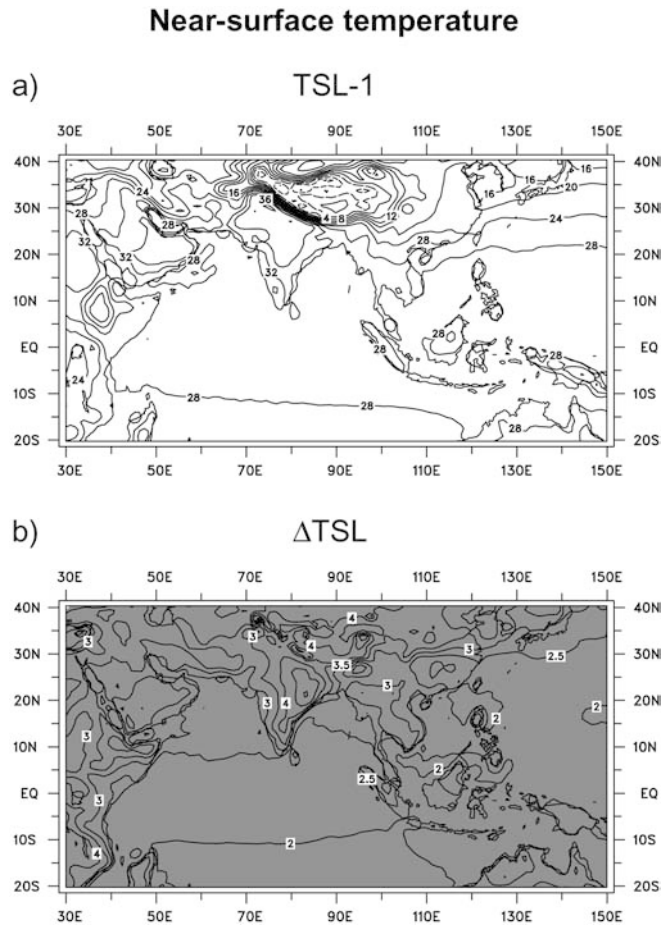
Fig. 3 Monthly mean (May) temperature in 2 m **a** for TSL-1 and **b** the difference between TSL-2 and TSL-1. The *shading* indicates the significance of the differences at the 95% level. Units are [° C]. The *contour interval* is 4 °C **a** and 0.5 °C **b**, respectively

trization of the soil processes (M03). Hence, the simulated temperature difference between the Indian Ocean and India is overestimated by 1 to 2 °C.

According to TSL, the anticipated increase in the greenhouse gas concentrations leads to an overall warming in Southeast Asia, and the warming is generally stronger over land than for the ocean areas (Fig. 3b). Over the tropical Indian Ocean, temperatures rise by 2 °C and over the northern Indian Ocean by 2.5 °C. In India, on the other hand, temperatures increase by 3 to 5 °C, with the largest warming occurring over the northeastern part of the Indian peninsula. These regional variations of the future warming cause a strengthening of the temperature difference between the Indian Ocean and central India by about 2.5 °C, suggesting an intensification of the Indian summer monsoon in the future. In fact, the onset of the Indian summer monsoon (defined via the very strong increase of the area-mean rainfall at the beginning of the monsoon season) occurs 7 to 10 days earlier in TSL-2 than in TSL-1 (not shown), consistent with a stronger meridional temperature gradient (e.g. Krishnamurti and Ramanathan 1982). Several coupled GCMs show a similar increase of the temperature difference between the Indian

Ocean and the land areas to the north in response to an increased level of CO_2, but the increase in the temperature difference is not a good predictor of the change in the monsoon rainfall (Douville et al. 2000). A possible explanation for the different model responses is that the enhanced meridional temperature gradient is secondary for producing changes in the monsoon rainfall as compared to SST anomalies in the Indian Ocean and in the tropical Pacific Ocean (Meehl and Arblaster 2002).

3.4 Eurasian snow cover

Another factor affecting the strength of the Indian summer monsoon is the Eurasian snow cover in the preceding spring, with a relatively weak monsoon flow following an excessive Eurasian snow cover and vice versa (e.g. Sankar-Rao et al. 1996). The excessive snow cover delays the springtime continental heating, weakening the thermal low over northern India and Persia and, by this, weakening the low-level monsoon flow (Douville and Royer 1996). Radiative processes, the turbulent transfers of heat and moisture, and hydrological processes are involved in the snow-monsoon relationship.

TSL-1 simulates an extensive snow cover over the Eurasian continent during spring (March to May), ranging from 1 cm at the western and southern edges to about 30 cm (water column) in north Siberia and in the far east, namely north of the Sea of Okhotsk and close to the Bering Sea (Fig. 4a). Compared to observations (Douville and Royer 1996), TSL-1 simulates the extent and depth of the Eurasian snow cover well, except for an underestimation of the snow cover in Europe and in the Caucasus region, as a consequence of a general warm temperature bias in these regions (May 2001). TSL-1 captures, on the other hand, the maximum snow depth in north Siberia very well, while the snow depth is overestimated north of the Sea of Okhotsk. Furthermore, TSL-1 simulates the snow cover in the Himalayas reasonably well, in particular the pronounced maximum (somewhat overestimated, though) in the southwestern part of the mountain range.

For the future, TSL predicts a considerable warming in Eurasia, exceeding 6 °C on an annual basis in northeast Asia (MR01). As a consequence, both the depth (Fig. 4b) and the extension of the Eurasian snow cover (Fig. 4c) are generally reduced in the future. The only regions with an increase in the snow depth are the Tundra areas in Northeast Asia located along the Kara Sea, the Laptev Sea and the East Siberian Sea (Fig. 4b). In these regions the melting caused by the warming is overruled by the accumulation of snow due to a significant increase in precipitation (MR01). Further, in these regions the temperatures stay below freezing despite the considerable warming of more than 6 °C. The strongest melting occurs, however, on the west coast of northeast Asia, caused by a relatively strong warming (> 3 °C) of the Bering Sea (May 1999). In the western part of the area, i.e. west of about 85°E, the southern edge of the

area covered with snow is moved northward by about 5° (Fig. 4c). In particular, the snow cover has disappeared in East Europe and the Balkans, as well as in southern Scandinavia. Further, the extension of the snow cover is reduced along the edge of the Himalayas, while the strongest reduction in the snow depth occurs in the southwestern part of the mountain range.

The pattern of the predicted change in the Eurasian snow depth is very similar to the pattern that according to Ferranti and Molteni (1999) leads to a strengthening of the Indian summer monsoon, both for the low-level monsoon flow and the monsoon rainfall. That is, the reduction in the snow depth is confined to the zone between 50 and 70°N and is most pronounced west of about 100°E. Therefore, also the predicted changes in the Eurasian snow cover suggest an intensification of the Indian summer monsoon in the future.

3.5 Walker circulation

The pattern of the predicted change of the SSTs in the tropical Pacific during the pre-monsoon season (March to May) includes some aspects of the SST anomalies during a typical El Niño event (Fig. 5). The strongest warming of up to 4 °C occurs on the equator centred around 110°W, and the area with higher temperatures extends further into the western Pacific. Just north and south of the area with the maximum increase, the warming is relatively weak, in particular to the south, where the temperatures actually are about the same in the future. Also near Indonesia and New Guinea, the warming is somewhat weaker. Apparently, the future warming in the tropical Pacific is strong (weak) in the regions with positive (negative) SST anomalies during a typical El Niño event. Such an event generally causes a relatively weak Indian summer monsoon (e.g. Webster and Yang 1992), suggesting that this particular pattern of the warming in TSL causes a weakening of the Indian summer monsoon in the future. The warming is rather strong (> 2.5 °C) in the Arabian Sea and the Bay Bengal but rather weak (< 2 °C) in the equatorial Indian Ocean and in the southern part of the Indian Ocean.

The changes of the SSTs in the tropical Pacific affect the convective activity and, by this, the release of latent heat, which then may alter the large-scale circulation over the tropical Pacific. The latter may also influence the large-scale circulation over the tropical Indian Ocean, since these two ocean basins are connected via the "Walker circulation" (e.g. Webster 1983).

Figure 6, therefore, shows the mean precipitation for the pre-monsoon season (March to May) as an indication for convective activity. According to this, TSL-1 simulates maximum rainfall (> 10 mm/d) over the "warm pool" in the western tropical Pacific and in the Indonesian region, extending further into the eastern tropical Pacific and the South Pacific (Fig. 6a). The strong convection in the Indonesian region and over the western tropical Pacific (extending into the eastern

Fig. 4 Seasonal mean (March, April and May; "MAM") snow depth (height of the equivalent water column) **a** for TSL-1 and **b** the difference between TSL-2 and TSL-1. Units are cm. **c** shows the change in the extent of the snow cover. The *red colour* indicates the areas, where the snow disappears in TSL-2, and the *blue colour* the areas with snow in both TSL-1 and TSL-2
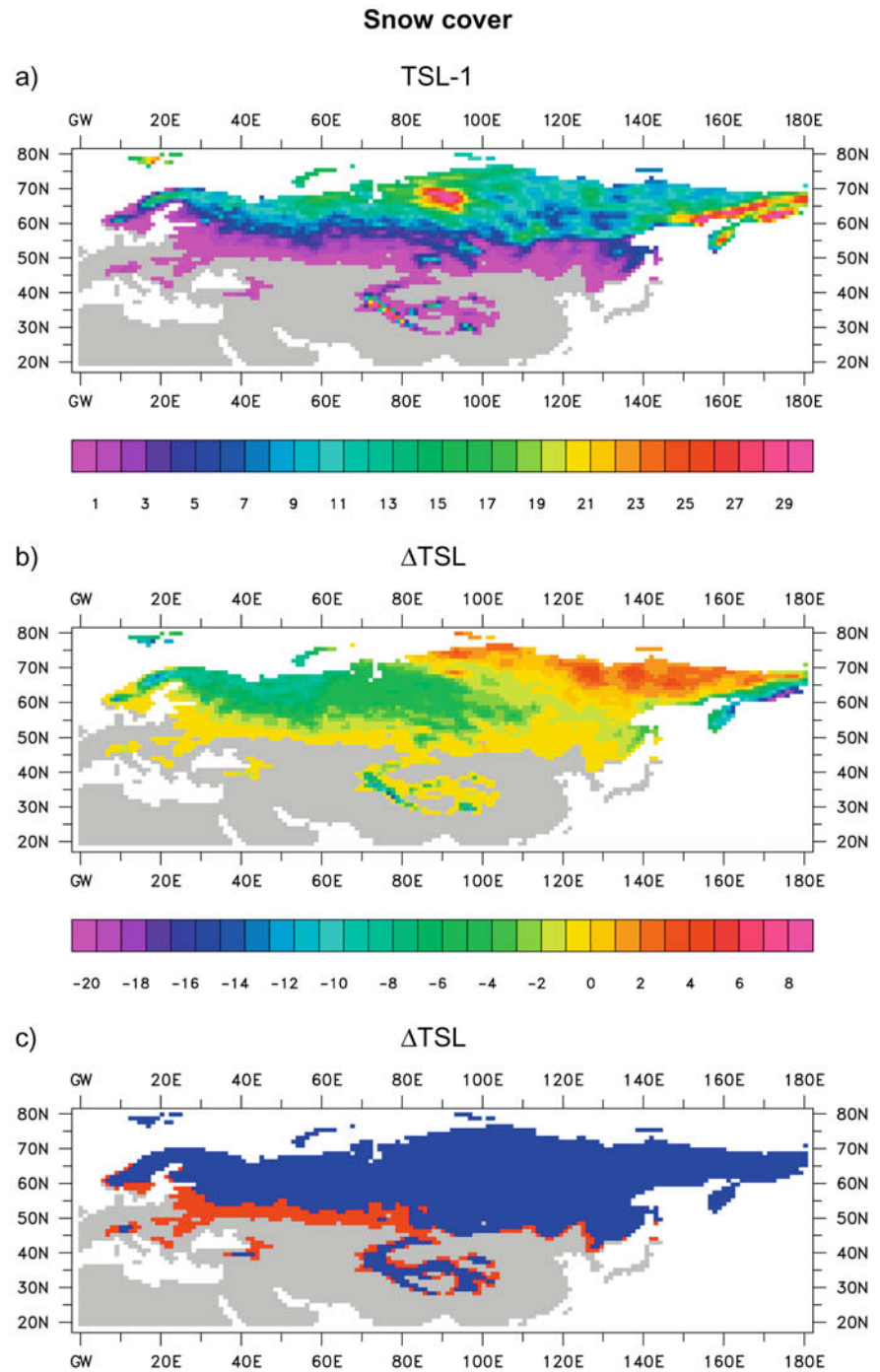
tropical Pacific) is organized within the Intertropical Convergence Zone (ITCZ), while the strong convective activity over the South Pacific is associated with the South Pacific Convergence Zone (SPCZ). During boreal spring, the ITCZ is located close to the equator over Indonesia and the western Pacific, but north of the equator over the eastern tropical Pacific. Compared to observations from the GPCP data set (Huffman et al. 1997) for the period 1979–1993 (not shown), TSl-1 simulates the location and structure of the ITCZ and the SPCZ very well, but generally overestimates the

magnitude by 10–20%. Part of this overestimation may, however, be accounted for by the lower resolution (2.5 °) of the observational data set.

The considerable future warming of the SSTs in the eastern tropical Pacific (see Fig. 5) leads to a considerable increase of the convective activity (corresponding to an increase in precipitation) in this region, accompanied by an equatorward shift of the eastern portion of the ITCZ (Fig. 6b). The maximum anomalies exceed 6 mm/d. Despite the warming, the convective activity is somewhat reduced within the SPCZ, as well as near

Fig. 5 Difference of the seasonal mean (MAM) sea surface temperature between TSL-2 and TSL-1. Units are °C
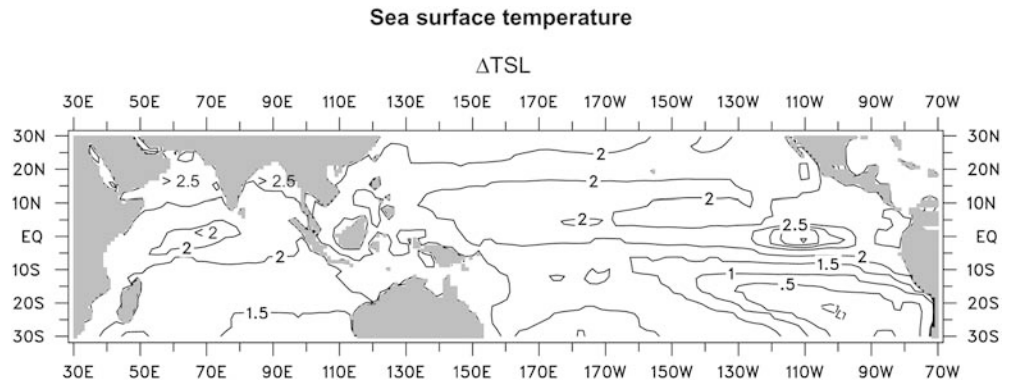
Fig. 6 Seasonal mean (MAM) daily precipitation **a** for TSL-1 and **b** the difference between TSL-2 and TSL-1. Units are mm/d. The *contour interval* is 2 mm/d
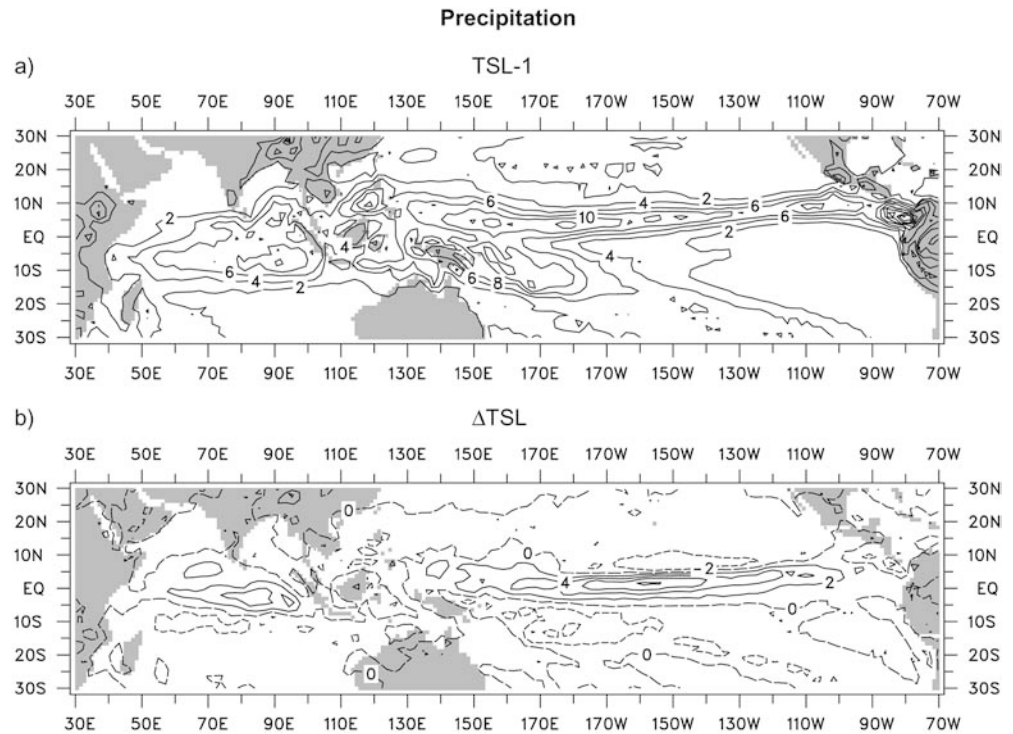
New Guinea and Indonesia and over the South China Sea (up to 4 mm/d). Over the tropical Indian Ocean, on the other hand, the convective activity is also markedly enhanced, indicted by rainfall exceeding 4 mm/d. Apparently, the relatively small SST anomalies of about 2 °C in the tropical Indian Ocean and in the tropical Pacific (centred at about 150°W), lead to only about 30% weaker increases in the convective activity as the rather strong warming of more than 4 °C in the eastern tropical Pacific (centred at about 110°W). This illustrates the importance of the mean SSTs for the increase in the convective activity, since the SST anomalies have the largest effect in the areas with the warmest mean SSTs. Along the equator, the predicted changes in the rainfall form a three-cell structure: two cells with enhanced convective activity (one over the Pacific, centred over the central and eastern parts of the basin, and one over the Indian Ocean) and one cell with reduced convective activity in the Indonesian region. These changes in the convection are accompanied by changes in the release of

latent heat, leading to a warming of the troposphere over the tropical Pacific and Indian Ocean and a cooling of the troposphere in the Indonesian region, respectively.

The non-uniform distribution of the heating in the tropics, i.e. the relatively strong heating over the land areas (Africa, Indonesia and New Guinea, and South America) and over the eastern Indian Ocean and western Pacific and the rather weak heating over the western Indian Ocean and the eastern Pacific, drives the zonal overturning along the equator, known as the Walker circulation. The structure of the Walker circulation can easily be depicted via the velocity potential in the lower (at 850 hPa) and in the upper troposphere (at 200 hPa), which are shown in Figure 7. The velocity potential indicates the divergent (and non-rotational) component of the flow and, by this, the regions with upward or downward motions. That is, the local maxima (minima) of the velocity potential indicate upward (downward) motions at the particular pressure level.

In agreement with observations, TSL-1 simulates the characteristic cells of the Walker circulation (e.g. Webster 1983): upward motions over central Africa, the Indonesian region and South America and compensating downward motions over the western Indian Ocean and the eastern Pacific (Fig. 7a, b). As a consequence, the low-level large-scale flow converges in the Indonesian region as well as over central Africa and South America but diverges over the eastern Indian Ocean and the western Pacific. This circulation pattern includes, for instance, the easterly trade winds over the equatorial central and western Pacific and westerly winds over the equatorial Indian Ocean. However, with the onset of the Indian summer monsoon the westerly winds shift north to the equator (see Fig. 1a). In the upper troposphere, on the other hand, the large-scale flow diverges over Indonesia and the continents but converges over the eastern Indian Ocean and the eastern Pacific. This is accompanied by easterly upper-level winds over the Indian Ocean and Indonesia and westerly winds over the central and eastern Pacific. The strongest upward motions (indicated by the highest (lowest) values of the velocity potential at 850 hPa (at 200 hPa)), which occur in the Indonesian region and over the western Pacific warm pool, are associated with the strongest convective activity (see Fig. 6a). The relatively strong downward motions over the eastern Pacific, on the other hand, are accompanied by relatively weak convective activity.

The rather strong warming in the eastern tropical Pacific alters the structure of the Walker circulation in the future. In the lower troposphere, the warming of more than 4 °C centred at about 110°W induces convergence of the low-level flow and, hence, an upward motion in this area (Fig. 7c). This large-scale circulation adjusts to this by an anomalous flow from South America and from the area south of the equator, centred at about the dateline. By the latter the warming in the eastern equatorial Pacific actually affects the SPCZ. Similarly, the relatively strong warming of more than 2.5 °C in the Arabian Sea induces low-level convergence in this region, and the circulation adjusts by an anomalous westward flow from the Indonesian region. The changes of the velocity potential at 850 hPa suggest only a weak connection between the changes in the SPCZ and the changes of the ITCZ in the Indonesian region, indicated by the relatively weak low-level convergence northwest of New Guinea.

In the upper troposphere, the low-level flow into the area over the eastern equatorial Pacific is compensated by an anomalous flow from this area into the SPCZ and Central America, respectively (Fig. 7d). The Indian Ocean and the Pacific, on the other hand, are connected via an anomalous westerly flow from the region south of India into the Indonesian region. Similarly to the lower troposphere, the changes in the Indonesian region and within the ITCZ are only weakly connected. Relatively weak upper-level divergence is found in the area south of New Guinea. Since these changes in the upper-level flow are consistent with the corresponding changes in the low-level flow (pointing into the opposite directions), they induce a cell structure with numerous closed cells.

An exception is, however, the area with large-scale divergence of the upper-level flow that is located on the equator between about 150–180°W. The distribution of the velocity potential at 200 hPa indicates an anomalous easterly flow across the equator from this area into the Indonesian region, but a corresponding counter part cannot be found in the lower troposphere (see Fig. 7c). This suggests that the increase in the release of latent heat, associated with enhanced convective activity, over the eastern equatorial Pacific takes place in different heights at different longitudes. Deep convection is actually suppressed in the eastern tropical Pacific, because a descending branch of the Walker circulation is located at these longitudes (see Fig. 7a). As a consequence, the rather strong surface warming between 110–120°W can only affect the lower troposphere. However, further to the west the surface warming on the order of 2 °C is able to induce additional deep convection, because this area is not affected by the descending branch of the Walker circulation (see Fig. 7b). This can also be seen from the change in precipitation, with the strongest increase at about 150°W (see Fig. 6b). This effect can also be seen over the Arabian Sea, where the relatively strong surface warming leads to enhanced low-level convergence (see Fig. 7c). In the upper troposphere, on the other hand, the area with the strongest convergence is shifted to the southeast (see Fig. 7d), where the conditions are more favourable for deep convection (see Fig. 7b).

The future changes in the Walker circulation suggest that the rather strong warming in the eastern tropical Pacific as well as in the Arabian Sea lead to a weakening of the eastern part of the Walker circulation. The anomalous divergence over the central tropical Pacific due to the future warming in the eastern tropical Pacific, for instance, leads to enhanced convergence in the Indonesian region. This, in turn, induces a reduction of the upper-level inflow into the Indian Ocean basin as well as a of the low-level inflow from the from the Indian Ocean basin and, by this, a weakening of the large-scale monsoon flow in the future. This effect is amplified by the anomalous upper-level divergence over the tropical Indian Ocean, caused by the warming over the Arabian Sea. These changes are consistent with the corresponding changes in precipitation, in particular for the upper troposphere, indicating that the changes in the Walker circulation are mainly driven by the changes in the latent heating associated with deep convection.

4 Hydrological cycle

4.1 Precipitation

The most important aspect of the Indian summer monsoon is the rainfall occurring in the monsoon season. Figure 8, therefore, shows among others the
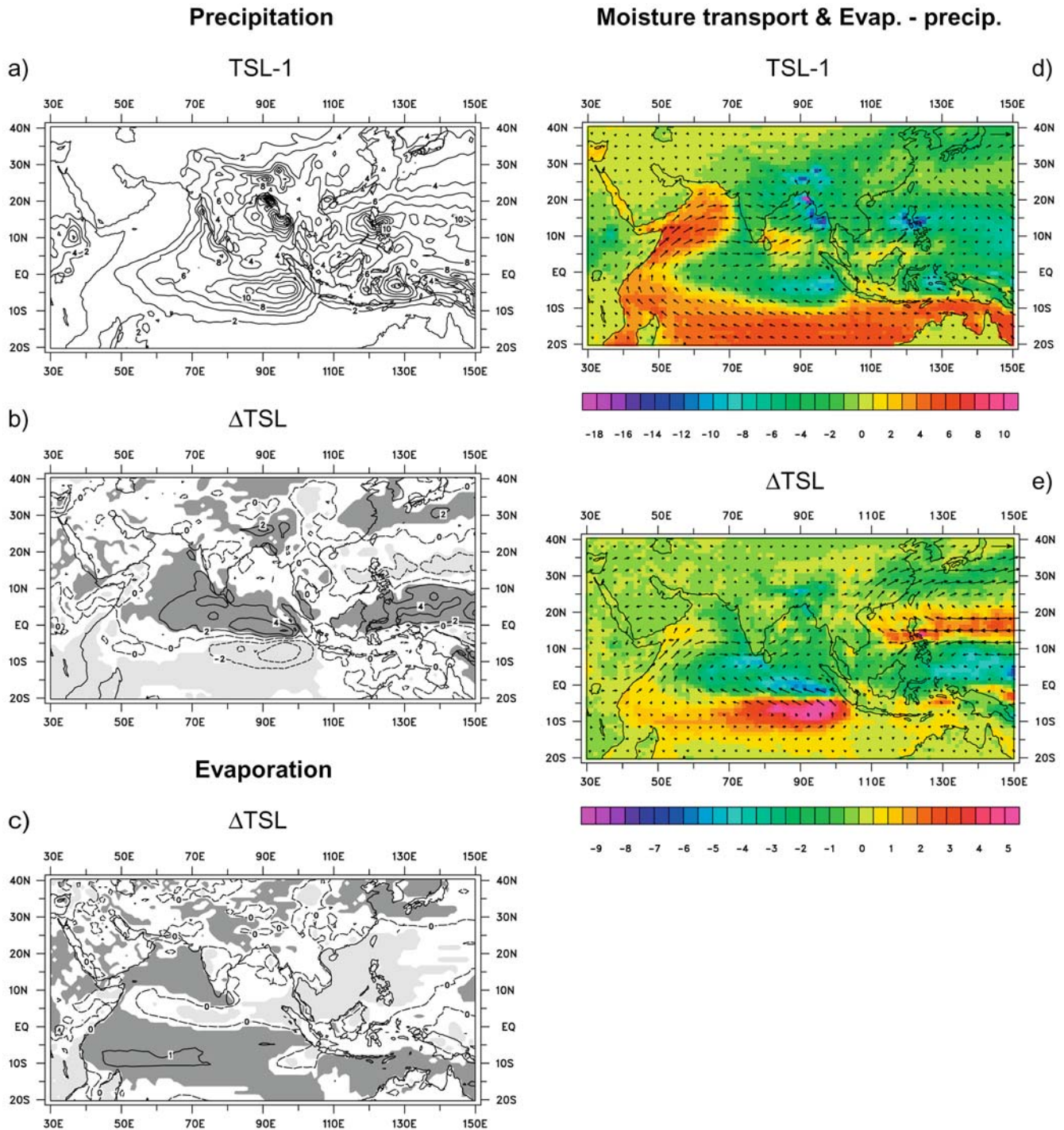
Fig. 7 Seasonal mean (MAM) velocity potential for TSL-1 at **a** 850 hPa and **b** 200 hPa. Further, the difference between TSL-2 and TSL-1 at **c** 850 hPa and **d** 200 hPa. Units are 10^6 m^2/s. The *contour interval* is **a** 1×10^6 m^2/s, **b** 2×10^6 m^2/s, **c** 0.2×10^6 m^2/s and **d** 0.4×10^6 m^2/s, respectively
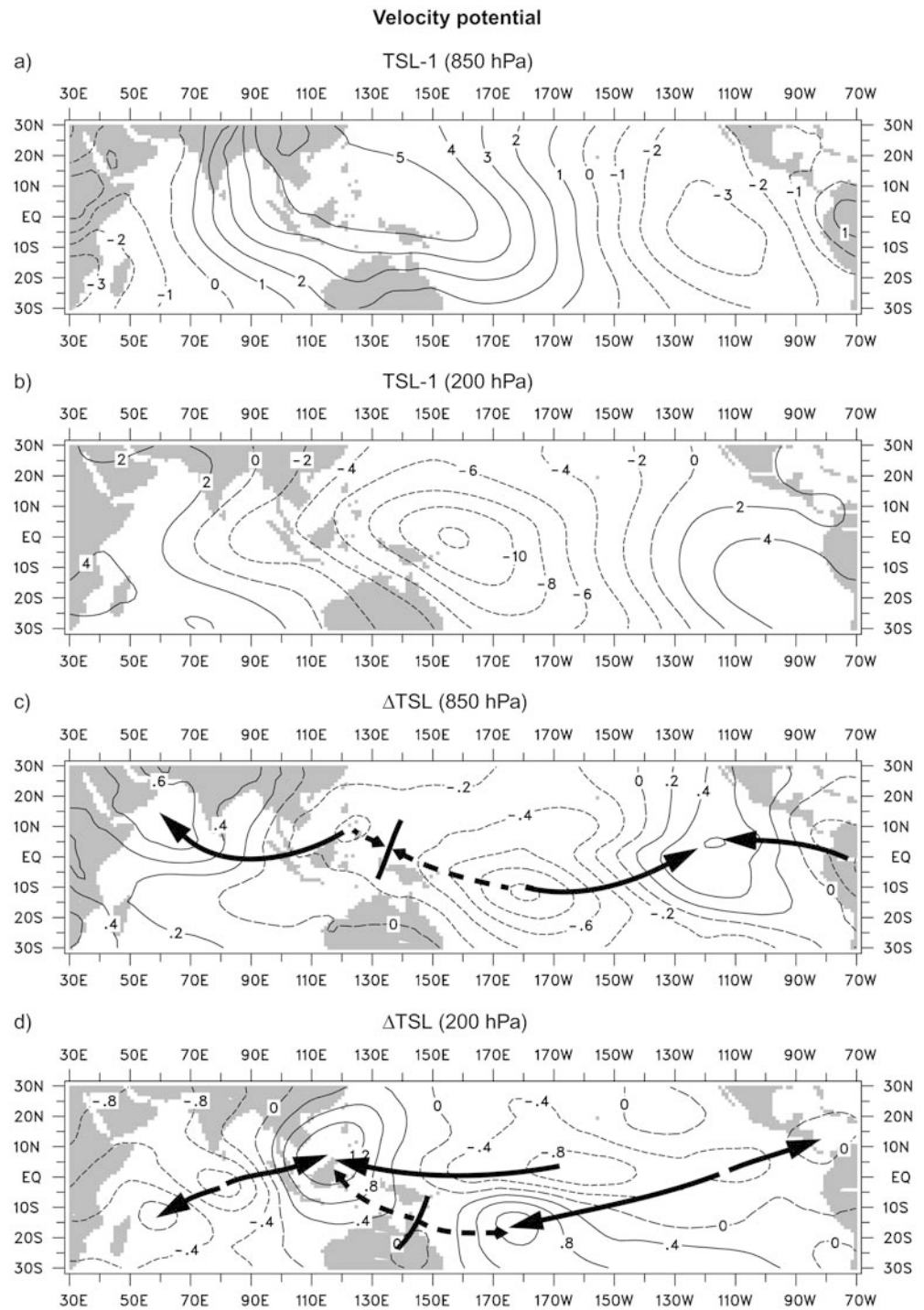
seasonal mean (June to September) distribution of daily precipitation.

Apparently, TSL-1 captures many aspects of the typical distribution of rainfall associated with the monsoon (Fig. 8a). These include the characteristic maxima near the west coast of the Indian peninsula, over the Bay of Bengal, and in Bangladesh and northeast India. In the western and southern parts of the Indian peninsula, on the other hand, precipitation is relatively weak. The strength of the maximum near the west coast of the

Indian peninsula is, however, considerably underestimated, depending on the observational data set by up to 50% (M03). Further, TSL-1 produces too much precipitation in the area southwest of Sri Lanka and to the west of Indonesia. Figure 8a reveals numerous regional details of the observed rainfall pattern in the Indian region, illustrating the importance of the high resolution of the GCM for providing regional climate information. In particular, the orographic nature of the precipitation in the Indian region is reproduced in TSL-1.

Precipitation

a) TSL-1

b) ΔTSL

Evaporation

c) ΔTSL

Moisture transport & Evap. - precip.

TSL-1   d)

ΔTSL   e)

Fig. 8 Seasonal means (JJAS) of **a** daily precipitation and **d** vertically integrated atmospheric moisture transport (*arrows*) and the difference between evaporation and precipitation (*E – P*; colours) for TSL-1. Further, the difference between TSL-2 and TSL-1 for **b** daily precipitation, **c** evaporation, and **e** vertically integrated atmospheric moisture transport (*arrows*) and *E – P* (*colours*). The *shading* indicates the significance of the differences at the 95% level (**b**, **c**). Units are mm/d and kg/(m × s) for the moisture transport, respectively. The *contour interval* is (**a, b**) 2 mm/d and **c** 1 mm/d respectively. The *arrows* in the *upper right corner* represent 800 kg/(m × s) **d** and **e** 200 kg/(m × s) **e**, respectively

For the future, TSL predicts an increase of precipitation in all the areas, where the rainfall is rather strong during the monsoon season, namely near the west coast of the Indian peninsula, over the Bay of Bengal, and in northeast India and Bangladesh (Fig. 8b). On the other hand, the amount of precipitation is reduced over much of the Indian peninsula, a region, where the monsoon rainfall is rather weak. These changes indicate an overall intensification of the monsoon rainfall in the future, caused by the anticipated increase in the greenhouse gas

concentrations. Rainfall is also increased over the equatorial and northern Indian Ocean, but reduced south of the equator. The latter indicates a northward shift of the convergence zone over the Indian Ocean.

Three distinct factors have been found that can contribute to the future changes in the distribution of rainfall over the Indian Ocean and the South Asian land areas: (a) the increase of the temperature difference between the Indian Ocean and the land areas to the north, (b) the warming of the SSTs in the Indian Ocean, and (c) the warming of the SSTs in the eastern tropical Pacific. Meehl and Arblaster (2002) found that these anomalies have different impacts on the distribution of the monsoon rainfall. The increased meridional temperature gradient causes a slight increase in precipitation over the South Asian land areas, while warm SST anomalies throughout the tropical Indian Ocean produce increased rainfall both over the Indian Ocean and over the South Asian land areas. However, warm SST anomalies restricted to the equatorial Indian Ocean lead to increased rainfall locally but decreased rainfall over the South Asian land areas. Warm SST anomalies in the eastern tropical Pacific, on the other hand, produce decreased rainfall over the Indian Ocean except near the equator, where rainfall is increased. At the same time, the monsoon rainfall is reduced in central India and over the Bay of Bengal. But according to Meehl and Arblaster (2002), the anomalous SSTs in the Indian and Pacific Ocean have larger impacts on the monsoon rainfall than the anomalous meridional temperature gradient over Asia.

In fact, the predicted future change in the rainfall distribution (see Fig. 8b) does appear to be a combination of the dominating effects of the SST anomalies in the Indian and Pacific Ocean. The warming throughout the tropical Indian Ocean with relatively small anomalies near the equator and very large anomalies in the Arabian Sea (see Fig. 5) itself would lead to increased rainfall over the Indian Ocean as well as over the South Asian land areas. In particular, the strong warming in the Arabian Sea would produce considerably more rainfall in southern India. The warming in the eastern tropical Pacific, on the other hand, would produce decreased rainfall in all the areas, where TSL predicts decreased rainfall for the future, i.e. over the southern part of the Indian Ocean and the Bay of Bengal as well as in central India. Further, these SST anomalies would produce increased rainfall over the Indian Ocean around the equator, where the future increase in precipitation is relatively strong. The fact that the warming in the eastern tropical Pacific Ocean has a strong impact on the future change in rainfall supports the main finding from the preceding section that the predicted changes in the large-scale flow are mainly accounted for by this warming. This, in turn, emphasizes the importance of the model's capability of realistically simulating the characteristics of the Walker circulation in order to give a plausible prediction of the changes in the Indian summer monsoon. Since the high-resolution version of ECHAM4 simulates the large-scale flow between the

Pacific and the Indian Ocean considerably better than the low-resolution version (see Sect. 3.1), TSL gives a more plausible prediction of the characteristics of the Indian summer monsoon due to the anticipated greenhouse warming than GHG.

4.2 Rainfall indices

As an alternative to the previously mentioned dynamically based indices for the Indian summer monsoon (see Sect. 3.2), the rainfall in the Indian region (8.5–30°N, 65–100°E) or the rainfall in India and Bangladesh (excluding the mountainous areas in northwest India; Sontakke et al. 1993), can be used to describe the strength of the Indian summer monsoon, focussing on the local aspects of the Indian summer monsoon.

According to Table 1, TSL-1 gives values of 5.88 mm/d for the area mean rainfall in the Indian region (IR-rain) and of 5.92 mm/d in India and Bangladesh (IB-rain). These values are somewhat smaller than observations because of the model's underestimation of rainfall near the west coast of the Indian peninsula. GPCP, for instance, yields values of 6.20 mm/d for IR-rain and of 7.10 mm/d for IB-rain for the period 1979–1993. For the future, TSL predicts a significant increase of both IR-rain ($\approx$13%) and IB-rain ($\approx$11%), indicating an intensification of the monsoon rainfall.

4.3 Atmospheric moisture transport

The future changes of precipitation in the Indian region (see Fig. 8b) are accompanied by corresponding changes in evaporation. TSL predicts, for instance, an increase in evaporation over the southern Indian Ocean (more precisely, south of the equator) and the Arabian Sea and a reduction over the northern Indian Ocean between the equator and 10°N (Fig. 8c). The increase over the southern Indian Ocean and the decrease in the band to the north is related to the northward shift of the tropical convergence zone in the future. Over the southern part of the ocean basin, the convective activity is reduced, leading to longer episodes without clouds and enhanced evaporation, while the opposite is the case over the northern part. Over the Arabian Sea, on the other hand, the relatively strong warming of the SSTs leads to enhanced evaporation, although rainfall and cloudiness also are increased in this area. Furthermore, evaporation is enhanced in north India, since the soil moisture content is increased in this area as a consequence of the increased rainfall.

The difference between evaporation and precipitation ($E - P$) defines a source or sink of atmospheric moisture at the surface, with positive values indicating a source and negative ones a sink, respectively. According to Fig. 8d, TSL-1 simulates moisture sources over the Indian Ocean south of about 10°S, near the African east coast and over the Arabian Sea. Another source of atmospheric moisture is located east of Sri Lanka.

Pronounced sinks of atmospheric moisture, on the other hand, are located over the equatorial Indian Ocean, near the west coast of the Indian peninsula, and over the northeastern part of the Bay of Bengal. But also in Bangladesh and northeast India evaporation is considerably stronger than precipitation. This tendency with precipitation exceeding evaporation is actually found over all the land areas in Southeast Asia. The areas with predominating precipitation are either associated with the tropical convergence zone (over the equatorial Indian Ocean) or with orographically forced rainfall (near the west coast of the Indian peninsula, over the northeastern part of the Bay of Bengal, and in northeast India and Bangladesh). The areas with predominating evaporation, on the other hand, are in general those with large-scale subsidence over the subtropical Indian Ocean.

Since the atmospheric moisture content is largest in the lower troposphere, the pattern of the atmospheric moisture transport (Fig. 8d) resembles to a large extent the wind pattern in the lower troposphere, i.e. at 850 hPa (see Fig. 1a). Over the Indian Ocean basin, atmospheric moisture is, hence, transported westward south of the equator and eastward to the north, with the direction changing in the vicinity of the African continent. The westerly moisture transport continues over the Arabian Sea and the Indian subcontinent, extending further into the eastern part of Southeast Asia. In the source regions of atmospheric moisture, i.e. the southern subtropical Indian Ocean, the western Indian Ocean, the Arabian Sea, and the area east of Sri Lanka, the atmosphere takes up moisture, and the prevailing winds transport most of this moisture to the Indian subcontinent and further into the eastern part of Southeast Asia.

Although the westerly winds at 850 hPa in the Indian region are only slightly enhanced in the future (see Fig. 1c), the westerly atmospheric moisture transport is considerable increased in this region, i.e. by about 20% relative to the present-day values (Fig. 8e). Apparently, over the Arabian Sea, the Indian peninsula and the Bay of Bengal the westerly changes of the winds in the middle and upper troposphere (see Fig. 1d) contribute to the strengthening of the vertically integrated atmospheric moisture transport. The northward shift of the tropical convergence zone over the eastern Indian Ocean is accompanied by a northward moisture flux from around 5°S towards and across the equator. Obviously, the future increase in the monsoon rainfall is due to the intensification of the atmosphere moisture flux into the Indian region, which, in turn, is related to an increase of the atmospheric moisture content in the future. The latter actually has two reasons. First, the general warming leads to an increase of the specific humidity in the atmosphere, also referred to as "precipitable water". And second, TSL predicts an increase in evaporation over the southern Indian Ocean and the Arabian Sea (see Fig. 8), leading to an additional source of atmospheric moisture in these regions (Fig. 8e). The increase in precipitation as a consequence of the enhanced

moisture transport may, however, be limited by a decrease in the water vapour recycling rate and in the precipitation efficiency (Douville et al. 2002).

Since the orographic forcing by the Western Ghats and the Himalayas is quite important for the spatial distribution of the monsoon rainfall, the simulation of rainfall as well as of the other components of the hydrological cycle is likely to depend on the horizontal resolution of the atmospheric GCM. In order to further investigate this, the simulation of the monsoon rainfall and of some related meteorological variables in GHG is compared with TSL.

In the Indian region, the simulation of the monsoon rainfall in GHG-1 (Fig. 9a) shows a number of differences from TSL-1 (see Fig. 8a), which actually reduce the quality of the simulation. GHG-1, for instance, considerably underestimates the amount of precipitation in those regions, where rainfall is strongly affected by the orographic forcing, such as near the west coast of the Indian peninsula, in the foothills of the Himalayas, and near the west coast of Burma and Thailand. As a consequence, GHG-1 does not captures the relatively small amount of precipitation east of the Western Ghats. The amount of precipitation is also underestimated in northeast India and Bangladesh, due to deficiencies in simulating the monsoon trough in GHG-1, including a severe underestimation of the inflow from the Bay of Bengal into northeast India and Bangladesh (see Fig. 2b). Further, GHG-1 is characterized by an additional erroneous rainfall maximum to the southwest of Sri Lanka, related to a northwestward extension of the convergence zone over the tropical Indian Ocean.

Also the future changes of the monsoon rainfall in the Indian region predicted in GHG (Fig. 9b) differ in several aspects from those predicted in TSL (see Fig. 8b). Both experiments are characterized by a northward shift of the convergence zone over the tropical Indian Ocean, but in GHG the area with increased rainfall covers almost the entire Indian region north of the equator. TSL, on the other hand, predicts reduced rainfall in the central part of the Indian peninsula and Pakistan. In northeast India, however, GHG shows a decrease in rainfall, while TSL is characterized by an increase. Apparently, in TSL the monsoon rainfall is enhanced in those regions, where it is generally strong, and decreased in those regions, where it is generally weak. GHG, however, does not show such regional differences but a uniform increase in rainfall in Pakistan, India and Bangladesh. As discussed, the future decrease of the rainfall in central India and over the Bay of Bengal predicted in TSL, is due to the future warming in the eastern tropical Pacific. But since the low-resolution version of ECHAM4 underestimates the large-scale flow between the Indian Ocean and the western Pacific (see Sect. 3.1), it also underestimates the impact of the warming in the Pacific on the monsoon rainfall, i.e. does not produce the decreased rainfall in central India and over the Bay of Bengal. In summary, the low-resolution model's deficiency in simulating the regional pattern of the monsoon rainfall and the large-scale flow between the

Precipitation

a) GHG-1

b) ΔGHG

Evaporation

ΔGHG c)

Evaporation - precipitation

ΔGHG d)
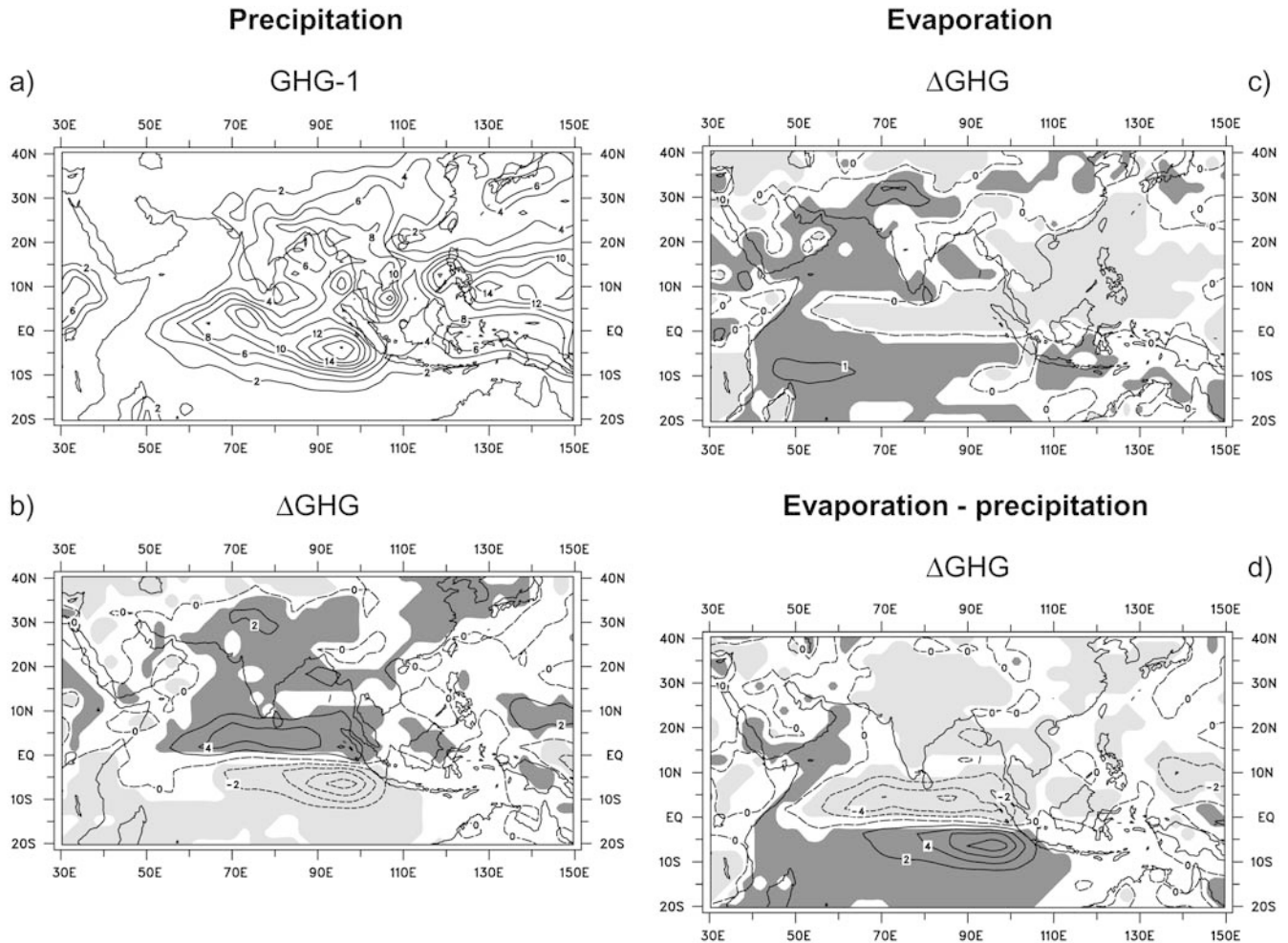
Fig. 9 Seasonal mean (JJAS) of daily precipitation **a** for GHG-1. Further, the difference between GHG-2 and GHG-1 for **b** daily precipitation, **c** evaporation, and **d** $E - P$. The *shading* indicates the significance of the differences at **b, c, d** the 95% level. Units are mm/d. The *contour interval* is 2 mm/d and 1 mm/d **c**, respectively

Indian Ocean and the western Pacific properly also affects the simulation of the regional pattern of the future change, impairing the plausibility of the changes predicted in GHG.

Consistent with the differences between the future changes in precipitation predicted in TSL and GHG, also the simulated changes in evaporation and $E - P$ differ between the two experiments. In contrast to TSL (see Fig. 8c), GHG predicts an increase in evaporation also in central India and over the Bay of Bengal (Fig. 9c). Apparently, part of the increased rainfall in these regions is produced locally in association with the enhanced evaporation. GHG predicts, however, a decrease or the source of atmospheric moisture in these region (Fig. 9d), since the increase in precipitation outweighs the increase in evaporation. As a consequence, the atmospheric moisture content is reduced over the Bay of Bengal and over the South Asian land areas, while TSL predicts an increase of $E - P$ and, hence, the atmospheric moisture content in central India and over the northern part of the Bay of Bengal as well as over the Tibetan plateau (see Fig. 8e).

4.4 River discharge

The river discharge is affected by large-scale changes in the different components of the hydrological cycle, i.e. precipitation and evaporation (discussed), but also by the changes in the soil water content and in the snow cover in the corresponding catchments. In order to investigate the river discharge in further detail, a hydrological discharge model (Hagemann and Dümenil 1997) has been applied to the three largest catchments in the Indian region. The discharge model distinguishes between the base, the overland, and the river flow. The latter two components are represented by a cascade of linear reservoirs, while the base flow is modelled by a single reservoir. The discharge model is forced by daily values of the surface runoff and drainage provided by the AGCM. The surface runoff is part of the overland water flow and the drainage part of the base flow, while the import from areas adjacent to the rivers feeds into the river flow. Anthropogenic impacts like dams, reservoirs or irrigation are not considered in the discharge model. The performance of the hydrological
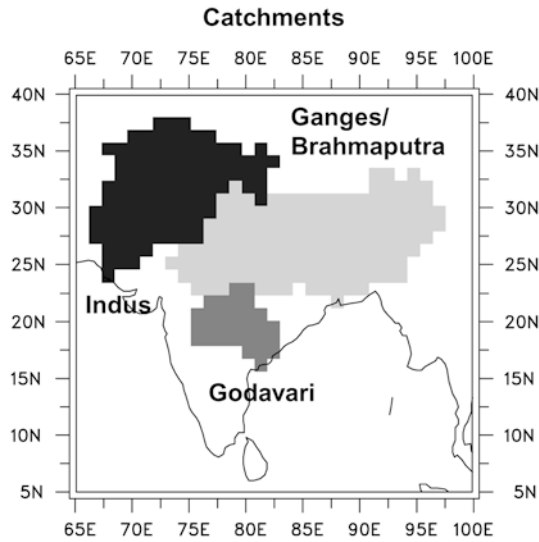
Catchments

Fig. 10 Three largest catchments in the Indian region

discharge model has been investigated in Hagemann and Dümenil (1997) for the global scale and in Hagemann and Dümenil (1999) for the Baltic Sea region. Further, Voss et al. (2002) have already applied the discharge model to data originating from TSL, focusing on the annual mean discharge from 14 of the world largest catchments, including the Ganges/Brahmaputra.

In this study, the three largest catchments in the Indian region are considered (Fig. 10). The Indus runs mostly through Pakistan into the Arabian Sea, but springs from the Tibetan plateau. The Ganges and Brahmaputra flow through northern India and northeast India, respectively, before joining in Bangladesh and running into the Bay of Bengal. Both rivers have various contributors springing from the Himalayas, and the Brahmaputra rises in this mountain range. The Godavari, on the other hand, flows through the northern central part of the Indian peninsula and, eventually, runs into the Bay of Bengal as well.

Figure 11 shows monthly mean values of the river discharge, both as observed and as obtained from the two time-slices, applying the hydrological discharge model. The observations have been provided by the Global Runoff Data Centre (Dümenil Gates et al. 2000). For all three rivers, the discharge undergoes a pronounced annual cycle, with a considerable discharge in the period July to October, in association with the Indian summer monsoon. Observed maxima actually occur in August, a few weeks later than the peak of the monsoon rainfall in July. Consistent with the marked monsoon rainfall in northeast India and Bangladesh,

for the Ganges/Brahmaputra (Fig. 11b) the discharge is 8 to 10 times stronger than for the Indus (Fig. 11a) and the Godavari (Fig. 11c), respectively. For the Ganges/Brahmaputra, the discharge obtained from TSL-1 has about the same order of magnitude as the
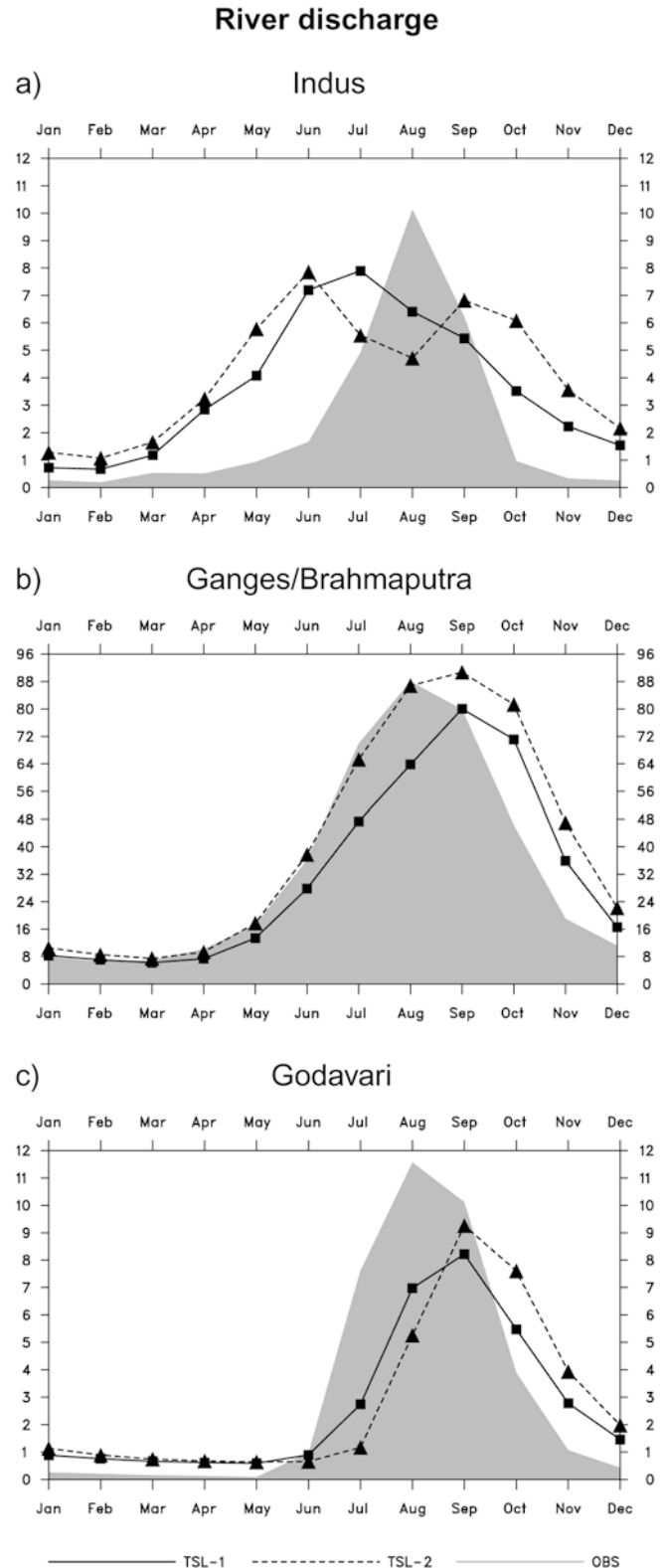
River discharge

Fig. 11 Monthly mean river discharge of three rivers in the Indian region: **a** Indus, **b** Ganges/Brahmaputra and **c** Godavari for observations (*shading*; Dümenil Gates et al. 2000), TSL-1 and TSL-2 (*curves*). Units are 10^3 m^3/s. Note the *varying scale*

observations, but its peak is one month delayed. The latter is also true for the Godavari, but in this case the maximum discharge is underestimated by about 25%. For the Indus, on the other hand, the simulated discharge peaks one month too early, and the maximum discharge is underestimated by about 20%. During spring, on the other hand, the strength of the discharge is considerably overestimated in TSL-1.

There are various possible reasons for the discrepancies between the simulated and the observed values of the river discharge. For the Ganges/Brahmaputra (Fig. 12b) and the Godavari (Fig. 12c), ECHAM4 actually simulates the shape of the annual cycle of precipitation in good agreement with observations (Hagemann and Dümenil Gates 2002). Therefore, the delayed peaks of the river discharge are not a consequence of corresponding temporal shifts of the annual cycle of the difference between precipitation and evaporation ($P - E$). Rather, the delays are presumably related to the relatively large storage of water in the ground in the respective catchments in July and August, in association with the unrealistically strong drying of the ground during the dry season in ECHAM4. This explanation is supported by the significantly too warm near-surface temperatures simulated by TSL-1 in these regions (M03). Another possible explanation is that the surface runoff as parametrized in the land-surface scheme is not efficient enough at transporting the water to the rivers. For the Godavari, the storage of water in the ground in July and August actually exceeds the maximum of the river discharge in September (Fig. 12c). The underestimation of the maximum discharge of both the Ganges/Brahmaputra and the Godavari in TSL-1, on the other hand, is caused by an underestimation of the maximum precipitation in July in the simulation (Hagemann and Dümenil Gates 2002).

Also for the Indus, TSL-1 captures the annual cycle of precipitation (Fig. 12a) and, hence, of $P - E$ in good agreement with observations (Shea and Sontakke 1995). A portion of the discharge of the Indus comes from the snowmelt in the Himalayas. According to TSL-1, the contribution from the snowmelt is as strong as the contribution from $P - E$, but peaks in May and June, while the largest values of $P - E$ occur in July and August. Due to the warm temperature bias of ECHAM4 in the Himalayas (M03), in TSL-1 the melting of the snow starts too early and, hence, the corresponding contribution to the river discharge occurs too early. This acceleration of the snowmelt also causes the underestimation of the maximum discharge of the Indus in TSL-1.

For the future, TSL predicts an increase of the maximum river discharge for both the Ganges/Brahmaputra (Fig. 11b) and the Godavari (Fig. 11c), still occurring in September. For the Ganges/Brahmaputra, the discharge is actually increased throughout the entire year, but in particular in July and August, that is during the monsoon season. As a consequence, also the annual mean discharge of the Ganges/Brahmaputra is enhanced by about 25% in the future (Voss et al. 2002). The discharge of the Godavari, on the other hand, is reduced in
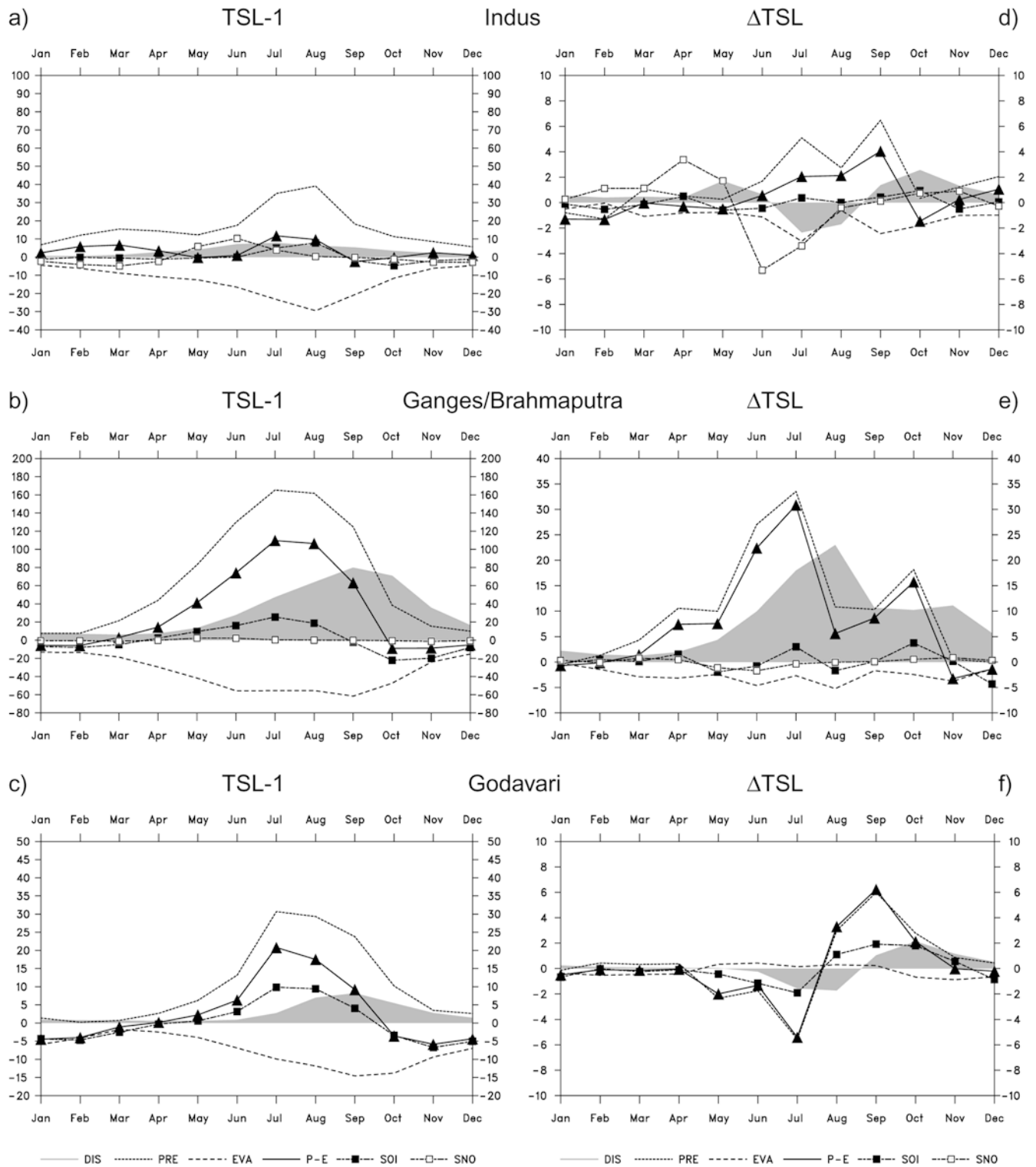
▶

Fig. 12 Monthly mean discharge (DIS) of three rivers (*shading*) in the Indian region as well as precipitation (PRE), evaporation (EVA; multiplied by −1), the difference between precipitation and evaporation ($P - E$), the storage of soil water (SOI), and the snowmelt (SNO) integrated over the corresponding catchments (*curves*) for TSL-1 (*left column*) and the difference between TSL-2 and TSl-1 (*right column*): (**a, d**) Indus, (**b, e**) Ganges/Brahmaputra and (**c, f**) Godavari. Units are [10^3 m^3/s]. Notice the *varying scale*

July and August but increased between September and December (Fig. 11c). For the Indus, however, TSL predicts a change in the shape of the annual cycle of the river discharge with two maxima, one in June and one in September and October (Fig. 11a). Further, the discharge of the Indus is generally enhanced in all months but July and August.

As to be seen in Fig. 12d, this change in the shape of the annual cycle of the Indus' discharge reflects two effects. First, in the future the melting of the snow starts already in April, as compared to June in TSL-1 (see Fig. 12a). And second, $P - E$ is increased between July and September with a maximum increase in September. The change in the annual cycle of the snowmelt accounts for the rather strong discharge of the Indus in June, while the change in $P - E$ (mainly following the change in precipitation) accounts for the rather strong discharge in September and October. For the Ganges/Brahmaputra, on the other hand, the future increase in the discharge mainly reflects a corresponding increase in precipitation, which is most pronounced in June and July (Fig. 12e). Also for the Godavari, the changes in the annual cycle of the discharge are mainly related to corresponding changes in the annual cycle of precipitation, which is considerably reduced between May and July and markedly enhanced between August and October (Fig. 12f). As a consequence, also the storage of the soil water is reduced between May and July and enhanced between August and October.

Apparently, the changes in the discharges of these three rivers are strongly affected by the changes in precipitation and evaporation in the corresponding catchments during the monsoon season (see Fig. 10). The strong increase of precipitation in the catchment of the Ganges/Brahmaputra during the monsoon season, particularly in June and July (Fig. 12e), coincides with an extensive significant increase of the mean precipitation in the Ganges valley, northeast India and Bangladesh (see Fig. 7b) as well as with a considerable reduction of $E - P$ (corresponding to an increase in $P - E$) in these areas (see Fig. 9b). Also in northwest India and northern Pakistan, the monsoon rainfall is significantly enhanced (see Fig. 7b), in accordance with the strong increase in precipitation in the catchment of the Indus between June and September (Fig. 12d). In the catchment of the Godavari, on the other hand, both precipitation and evaporation are slightly reduced during the monsoon season (see Figs. 7b and 8, respectively), so that $E - P$ is hardly changed on a seasonal mean basis (see Fig. 9b). This is, however,

River discharge

a) TSL-1 Indus ΔTSL d)

b) TSL-1 Ganges/Brahmaputra ΔTSL e)

c) TSL-1 Godavari ΔTSL f)

DIS ·········· PRE ------ EVA —— P–E ---■--- SOI ---□--- SNO

somewhat misleading, since precipitation in the corresponding catchment actually is affected by the greenhouse warming, namely by a decrease in precipitation between May and July and an increase between August and October (Fig. 12f).

5 Interannual variabilty

According to the latest IPCC report (Houghton et al. 2001), the future increase in the mean monsoon rainfall

is likely to be accompanied by an increase in its interannual variability. And, in fact, some recent studies (Hu et al. 2000; Lal et al. 2000; Meehl and Arblaster 2003) have reported on an increase in the interannual variability of the monsoon rainfall in association with an overall increase of the monsoon rainfall, but have assigned it to different causes. While Hu et al. (2000) related the increase in the interannual variability to a corresponding increase of the SST variability in the tropical Pacific Ocean, Meehl and Arblaster (2003) assigned it primarily to warmer mean SSTs in the tropical Pacific Ocean, accompanied by enhanced evaporation variability. Therefore, it is interesting to investigate what kind of future changes TSL predicts for the interannual variability of the Indian summer monsoon and what mechanisms cause such changes.

As for the different monsoon indices, TSL predicts a considerable increase in the interannual variability of both U-shear and IR-rain in the future, i.e. for U-shear the variance is increased by a factor of 2.86 and for IR-rain by a factor of 1.83 (Table 1). For the two other indices, i.e. V-shear and IB-rain, the increase is only about 20%. Apparently, the meridional component of the monsoon flow, i.e. the local Hadley circulation, is not as strongly affected by the change in the variability as the zonal component of the flow. As a consequence of the dominant coupling between U-shear and IR-rain (correlation coefficients: 0.40 and 0.73 for TSL-1 and TSL-2, respectively; Table 2) on one hand and between V-shear and IB-rain (correlation coefficients: 0.69 and 0.71) on the other, the relatively small (large) increases in IB-rain (IR-rain) may to a large extent be related to the corresponding rather small (large) increases in the interannual variability of the local Hadley circulation (Walker circulation). The fact that the correlation between IR-rain and U-shear is considerably enhanced in the future (0.73 versus 0.40) but not the correlation between IB-rain and V-shear (0.71 versus 0.69), suggests that the robustness of the connection between the Indian rainfall and the monsoon flow may well depend on the strength of the variations of the flow.

As for the local changes, TSL predicts an increase in the interannual variability of the monsoon rainfall over all of the Indian region, except for the southern Indian Ocean and a few smaller regions, such as over the northern part of the Indian peninsula, over the western part of the Bay of Bengal, and in parts of the Himalayas (Fig. 13a). In these areas also the mean monsoon rainfall is reduced (see Fig. 8b), indicating a connection between the future change in the mean rainfall and the future change in its variability. In the region with the strongest increase in the overall rainfall, i.e. around the equator, about half of the increase in the variance is actually accounted for by the increase in the mean rainfall, while in the other regions with increased variability the increases in the overall rainfall only are of minor importance. Consistent with the increased variability of the monsoon rainfall, the intertannual variability of the zonal wind component in the lower troposphere is enhanced over the Arabian Sea, in particular within the Somali jet, over India and over Southeast Asia (Fig. 13b). The interannual variability of the meridional wind component, on the other hand, is mainly increased over India and Southeast Asia as well as over the Indian Ocean between about 5°S and 10°N, indicating enhanced interannual variability of the cross-equatorial flow (Fig. 13c).
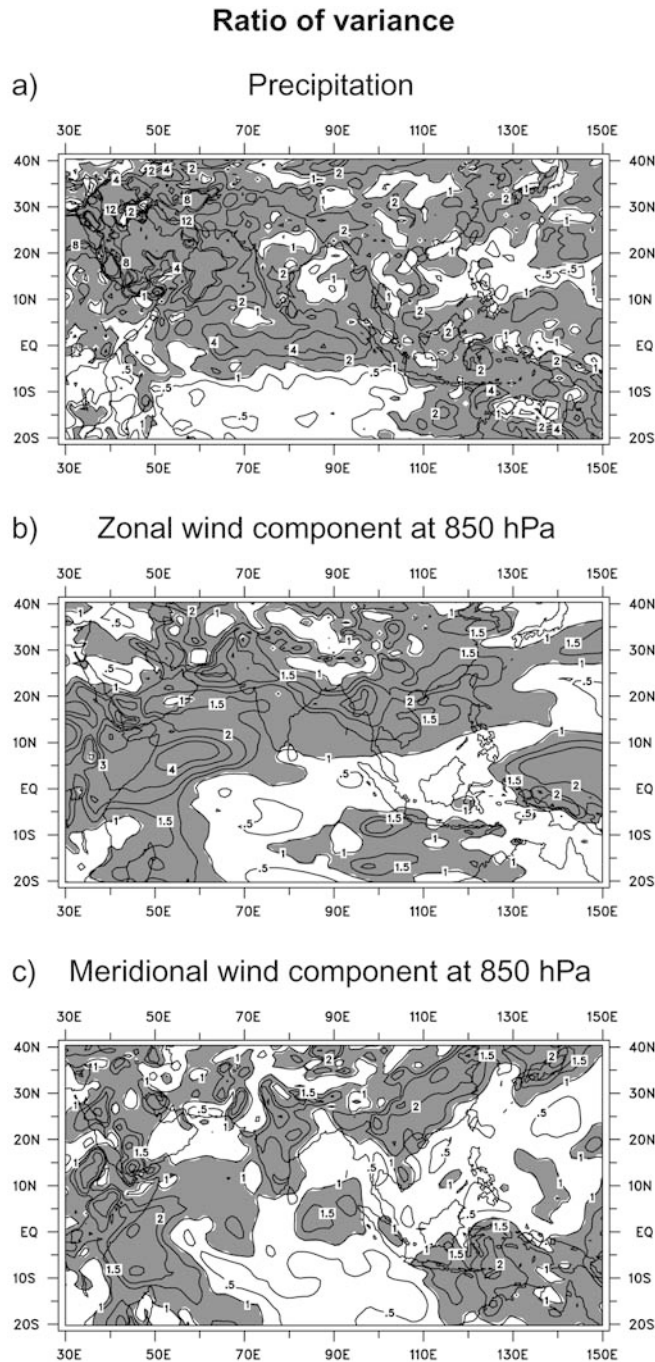
Since, however, the interannual variability of the SSTs in the Indian Ocean is reduced in the future (not shown), the enhanced variability of the Indian summer monsoon cannot be related to the lower boundary forcing over the Indian Ocean basin but rather to other processes. Meehl and Arblaster (2003), for instance, explained the increased variability of the South Asian monsoon rainfall as the consequence of warmer SSTs in the tropical Pacific Ocean, leading to enhanced evaporation variability. Also warmer SSTs in the tropical and northern Indian Ocean contributed to the increased interannual variability, but to a considerably smaller extent. These two mechanisms may also be at work in TSL, which predicts a warming in both the tropical Pacific and the Indian Ocean (see Fig. 5). Hu et al. (2000), on the other hand, speculated that the increase in the interannual variability of the summer monsoon could be related to a corresponding enhancement of the interannual variability of the SSTs in the tropical Pacific, but did not further explore their hypothesis. Since the variance of the SSTs in the central and eastern tropical Pacific (Niño-3 region) is increased by a factor of 3.19 between TSL-1 and TSL-2 (Table 3), it seems worthwhile to investigate this hypothesis in further detail.

The climate change simulation that has provided the lower boundary forcing for TSL is characterized by a general increase in the interannual variability of the SSTs in the Niño-3 region due to greenhouse warming (Timmermann et al. 1999). There is also a tendency of strong La Niña events becoming more frequent in the future. The future changes in ENSO interannual variability can, however, differ from model to model (Cubasch et al. 2001). In models that show increases, this is related to an increase in the intensity of the thermocline in the tropical Pacific. Superimposed on the long-term trend in GHG are, however, marked variations on decadal time scales. The 25-years period centred around 1972, for instance, is characterized by rather low inter-

Table 2 Correlations between monsoon indices

	U-shear	V-shear	IR-rain	IB-rain
U-shear		–0.23	0.40*	0.26
V-shear	0.07		0.42**	0.69***
IR-rain	0.73***	0.55***		0.72***
IB-rain	0.55***	0.71***	0.85***	

See text for the definitions of the indices. The upper triangle includes the correlation coefficients between the different monsoon indices for TSL-1 and the lower triangle those for TSL-2. ***, ** and * indicate differences exceeding a 99.9%, a 97.5% and a 95% level of significance, respectively

Ratio of variance

a) Precipitation

b) Zonal wind component at 850 hPa

c) Meridional wind component at 850 hPa

Fig. 13 Ratio of the interannual variance between TSL-2 and TSL-1 for the seasonal mean (JJAS) values of **a** daily precipitation, **b** the zonal, and **c** the meridional wind component at 850 hPa. The *shading* indicates ratios exceeding 1. The contours shown are at **a** 0.5, 1, 2, 4, 8, and 12 and **b** 0.5, 1, 1.5, 2, 3, 4, 6, 8, and 12, respectively

Table 3 Correlations with Niño-3 index

	STD (°C)	U-shear	V-shear	IR-rain	IB-rain
TSL-1	0.84	–0.34	0.03	0.21	–0.05
TSL-2	1.50	–0.78***	–0.49**	–0.83***	–0.77***
EXPL VAR TSL-2 (%)		60.8	24.0	68.9	59.3

P Correlation coefficients between the Niño-3 index (SST-anomalies in [5°S–5°N, 210–270°E]) in the period June to September and the different monsoon indices for TSL-1 and TSL-2. ***, ** and * indicate differences exceeding a 99.9%, a 97.5% and a 95% level of significance, respectively. Also, the interannual variations of the Niño-3 index for the two time-slices ("STD"). The ratio of variance between TSL-2 and TSL-1 is 3.19. Further, fraction of the variance of the different monsoon indices explained by the variations of the Niño-3 index for TSL-2

by very strong variations (Fig. 14b). During the other halves of two periods the interannual ENSO variability has about the same magnitude. Also the strength of the Indian summer monsoon is characterised by variations on decadal time scales, illustrated by corresponding variations of the different monsoon indices. In contrast to the Niño-3 index, the interannual variations of all four monsoon indices are rather weak (about 0.5 standard deviation) in the period 1985–1999 (Fig. 14a). Only IR-rain shows a steady decrease of the interannual variability before 1985, while the other indices vary around a value of 1 standard deviation. In TSL-2, on the other hand, all four monsoon indices follow the Niño-3 index and show enhanced interannual variability after 2074 (Fig. 14b). In particular *U*-shear and IR-rain are characterized by a similar abrupt increase in the interannual variability around 2075, while for *V*-shear and IB-rain the interannual variability increases gradually after 2074, reaching values of about 1 standard deviation not before 2082 and maximum values of about 1.5 standard deviation at the end of the period. For IB-rain, however, similar values of the interannual variability also occur at the beginning of TSL-1. *U*-shear and IR-rain, on the other hand, exceed values of 1.5 and 1 standard deviation, respectively, already around 2072.

As for the impact of the ENSO phenomenon on the Indian summer monsoon, the two time-slices give very different results (Table 3). In TSL-1 none of the four monsoon indices is significantly correlated with the Niño-3 index, and IR-rain even has a positive correlation of 0.21. In TSL-2, however, all four monsoon indices are significantly correlated with the Niño-3 index, and the correlations are negative, as one would expect according to observations (e.g. Rasmusson and Carpenter 1983; Webster and Yang 1992) and other modelling studies (e.g. Ju and Slingo 1995; Lau and Nath 2000). The impact of the ENSO phenomenon on *V*-shear and, hence, the local Hadley circulation is somewhat weaker (24% of the variance are explained by variations of the Niño-3 index) than on the three other indices, for which between 60-70% of the variance are explained by variations of the Niño-3 index.

annual ENSO variability but the 20-years period centred around 2085 with very strong variability (Timmermann et al. 1999).

Obviously, these variations also affect the two periods of TSL. The first half of the period 1970–1999 is characterized by rather weak variations of the Niño-3 index (Fig. 14a) but the second half of the period 2060–2089
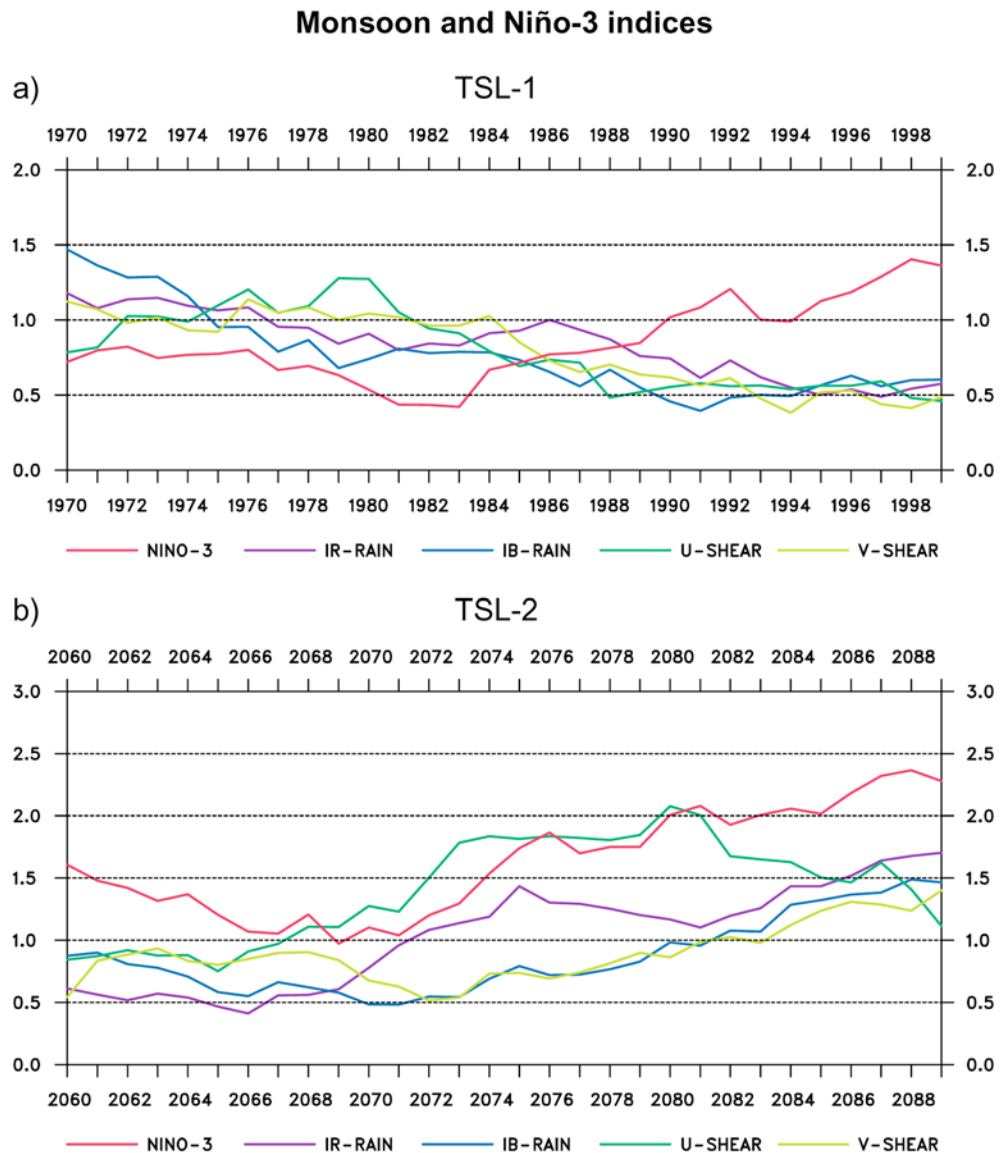
Fig. 14 Low-pass filtered (9-years running mean) interannual standard deviations of the different monsoon indices and the Niño-3 index (JJAS) for **a** TSL-1 and **b** TSL-2. For the definition of the Niño-3 index see Table 3. The values are normalized by the overall interannual standard deviation of the individual indices for TSL-1 (see Tables 1 and 3)


The fact that the correlations with the Niño-3 index are very weak in TSL-1 is quite unexpected. One possible explanation is that ECHAM4 does not properly simulate the impact of interannual variations of the SSTs. A closer look at an AMIP-type simulation with ECHAM4 at a horizontal resolution of T106 for the period 1979–1993 (M03) reveals that ECHAM4 actually is able to capture the interannual variations of the monsoon indices, in particular for the rainfall. For IR-rain and IB-rain, the correlations with the GPCP data are 0.69, while for U-shear and V-shear the correlations with ERA are only 0.31 and 0.24, respectively. Another possible explanation are decadal variations of the correlations with the Niño-3 index. TSL-1 shows indeed such variations for the different monsoon indices (Fig. 15a). All indices except IR-rain are negatively correlated with the Niño-3 index in a 15-years period centred around the 1980's, and for U-shear the negative correlations are relatively strong after about 1984. This is also the period

of a relatively strong interannual variations of the SSTs in the tropical Pacific (see Fig. 14a). TSL-2, on the other hand, shows a steady strengthening of the correlations with the Niño-3 index throughout the entire period for all the monsoon indices except for V-shear (Fig. 15b). After about 2072, that is the period with very strong interannual ENSO variability (see Fig. 14b), the correlations with the three monsoon indices exceed a value of –0.80.

These results suggest that the impact of the ENSO phenomenon on the Indian summer monsoon is influenced by the strength of the interannual variations of the SSTs in the tropical Pacific. Only when the SST anomalies exceed a certain threshold, the Indian summer monsoon responds systematically, with El Niño (La Niña) events leading to weak (strong) summer monsoons. But the results also indicate that this threshold is lower for the future climate than for the present-day climate. Although the interannual ENSO

Fig. 15 Correlation coefficients between the Niño-3 index (JJAS) and the four monsoon indices for 11-year sliding windows centred at the year indicated on the abscissa for **a** TSL-1 and **b** TSL-2
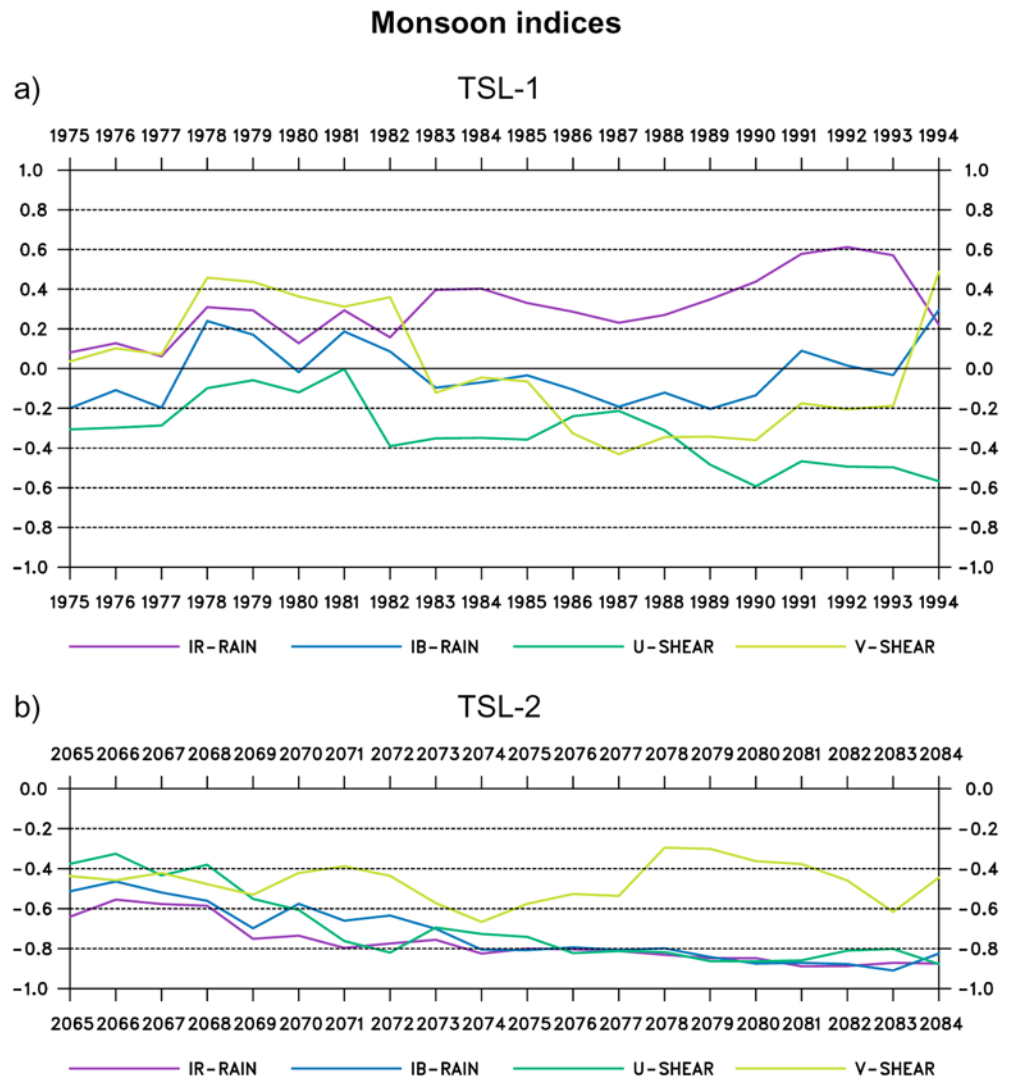
variations have about the same strength in the second half of the period 1970–1999 and in the first half of the period 2060–2089, the response to the ENSO phenomenon is much more robust during 2060–2074. This is probably a consequence of the general future warming (MR01), leading to a marked increase of the atmospheric moisture content. Therefore, the anomalous diabatic heating associated with individual ENSO events and, hence, the effect of the SST anomalies on the atmospheric circulation are enhanced in the future.

As for the local impact of the ENSO phenomenon on the Indian summer monsoon, TSL-2 shows a marked reduction (increase) of the rainfall over most of the Indian region during El Niño (La Niña) events (Fig. 16a). The strongest impact occurs off the west coast of the Indian peninsula, where more than 60% of the interannual variance are explained by variations of the Niño-3 index. The opposite behaviour with increased (reduced) rainfall during El Niño (La Niña) events is found on the equator, in particular west of Sumatra. The reduction (increase) of the rainfall in the Indian region is related to a weakening (strengthening) of the westerly winds over the Arabian Sea, the southern part of the Indian peninsula and the Bay of Bengal (Fig. 16b), leading less (more) moisture into the Indian region. These changes are accompanied by a reduction (increase) of the predominantly easterly winds further to the north. Variations of the Niño-3 index actually explain up to 80% of the interannual variability of the Somali-jet. During El Niño events the northerly flow over the Indian peninsula is enhanced and extending over the Bay of Bengal (Fig. 16c), leading to a reduction of the predominately southerly winds in this region and, hence, of the inflow of moist air from the Bay of Bengal into eastern India and Bangladesh. During La Niña events, on the other hand, the situation is reversed with an enhanced inflow of moist air into eastern India and Bangladesh.

6 Summary and conclusions

In this study the potential impact of the anticipated increase in the greenhouse gas concentrations on different aspects of the Indian summer monsoon is investigated,

Variance expl. by Niño-3 index - TSL-2

a) Precipitation

b) Zonal wind component at 850 hPa

c) Meridional wind component at 850 hPa
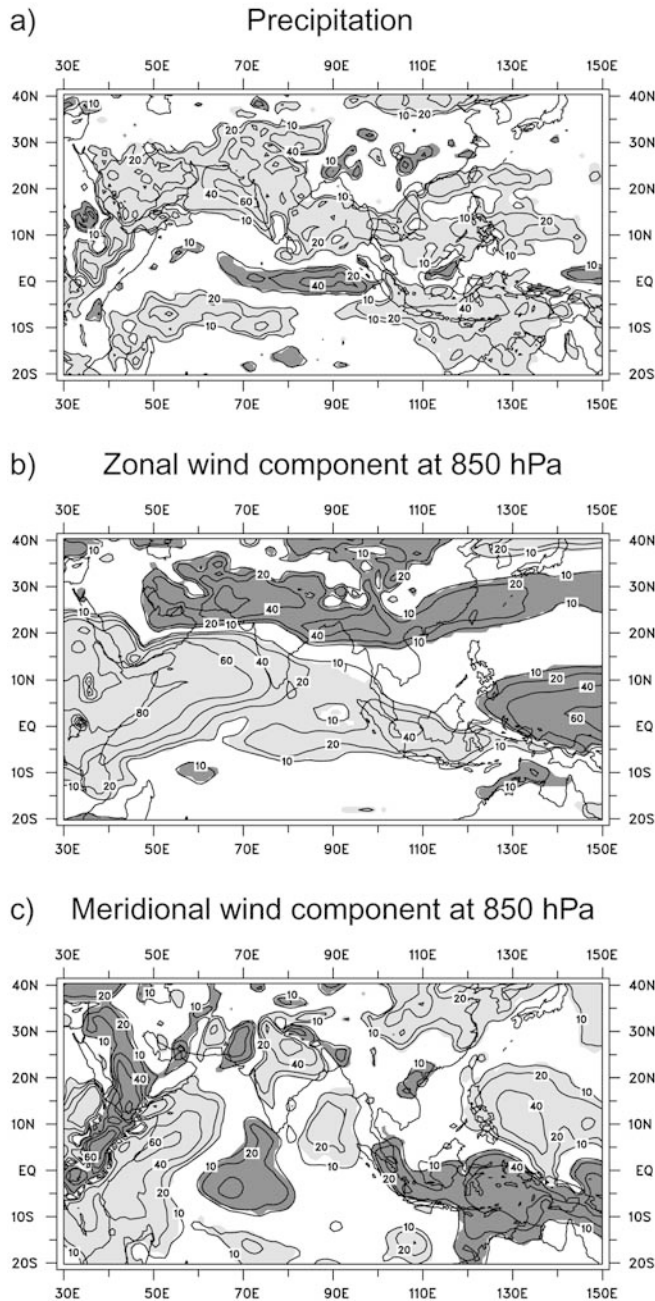
Fig. 16 Fraction of the interannual variance of the seasonal mean (JJAS) values of **a** daily precipitation, **b** the zonal, and **c** the meridional wind component at 850 hPa explained by the Niño-3 index for TSL-2. The *shading* indicates the significance at the 90% level, i.e. the *heavy* (*light*) shading for positive (negative) correlations with the Niño-3 index. Units are [%]. The *contours* shown are at 10, 20, 40, 60, and 80%

focussing on the role of the mechanisms leading to these changes. Both changes in the mean aspects of the Indian summer monsoon and changes in its interannual variability are considered. This is done on the basis of a time-slice experiment (TSL), which has been performed with the ECHAM4 AGCM at a high horizontal

resolution of T106. TSL consists of two 30-year simulations, one representing the present-day climate (period: 1970–1999) and one representing the future climate (period: 2060–2089).

TSL predicts an intensification of the mean rainfall associated with the Indian summer monsoon as a consequence of the anticipated increase in the greenhouse gas concentrations. For the large-scale flow, on the other hand, TSL is characterized by a weakening of the monsoon circulation in the upper troposphere and only little change in the lower troposphere. Observations also indicate a weakening of the large-scale aspects of the Indian summer monsoon over the period 1958–1998 (Stephenson et al. 2001), while the all-India rainfall ("AIR") shows only little evidence of a change in recent historical observations (Rupa Kumar et al. 1992). When Stephenson et al. (2001), however, removed the dynamical contribution from the observed AIR, they found a clear increasing trend in the non-dynamical residual of AIR over the last four decades of the twentieth century.

The future intensification of the rainfall associated with the Indian summer monsoon is related to an intensification of the atmospheric moisture transport into the Indian region, which, in turn, is due to an increase in the atmospheric moisture content. The latter has two reasons: first, an increase of the specific humidity in the atmosphere due to the general warming and, second, additional sources of atmospheric moisture due to enhanced evaporation over the southern Indian Ocean and the Arabian Sea.

As for the future changes in the large-scale flow associated with the Indian summer monsoon, several competing mechanisms are at work. The weakening of the monsoon flow is caused by the pronounced warming of the SSTs in the central and eastern tropical Pacific and the associated alterations of the Walker circulation. The latter is characterized by an anomalous westerly flow from the Indian Ocean basin into the Indonesian region in the upper troposphere and an anomalous easterly flow from the Indonesian region towards the Arabian Sea in the lower troposphere. TSL, however, also predicts a future increase of the temperature difference between the Indian Ocean and the land areas to the north as well as a future reduction of the Eurasian snow cover in spring. By themselves, these two mechanisms lead to an intensification of the Indian summer monsoon in the future (e.g. Krishnamurti and Ramanathan 1982; Sankar-Rao et al. 1996). Apparently, these two mechanisms compensate for the weakening of the monsoon flow induced by the warming over the tropical Pacific in the lower, but not in the upper troposphere. As a consequence, the low-level monsoon flow shows only little change in the future. These findings are supported by a recent study by Meehl and Arblaster (2002), according to which anomalous SSTs in the tropical Indian Ocean and the tropical Pacific lead to a larger response of the monsoon compared to the anomalous meridional temperature gradient over Asia. In particu-

lar, warm SST anomalies in the eastern tropical Pacific produce decreased rainfall in central India and over the Bay of Bengal.

TSL also predicts a future increase in the interannual variability of both the rainfall associated with the Indian summer monsoon and of the large-scale flow. A major part of this increase is accounted for by variations of the SSTs in the central and eastern tropical Pacific, typically associated with the ENSO phenomenon. The latter has two causes: first, the future climate is characterized by an increase in the magnitude as well as in the frequency of SST-variations in this region and, second, the effect of these SST anomalies on the Indian summer monsoon may be amplified. Due to the general future warming, the atmospheric moisture content is increased and, hence, the diabatic heating associated with the anomalous deep convection is amplified. Furthermore, part of the enhanced interannual variability of the monsoon rainfall may be the consequence of warmer SSTs in the tropical Pacific, leading to enhanced evaporation variability (Meehl and Arblaster 2003).

The simulation of the Indian summer monsoon by ECHAM4 is considerably improved at the high horizontal resolution of T106 compared to the low-resolution (T42) version of the model. This is not only the case for the regional maxima of the monsoon rainfall, which are strongly affected by the Western Ghats and the Himalayas, but also for the large-scale flow over the Indian Ocean and the South Asia land areas. In particular, the low-resolution version of ECHAM4 significantly underestimates the atmospheric flow between the western Pacific and the Indian Ocean. Therefore, it also underestimates the impact of the future warming in the tropical Pacific on the large-scale circulation over the Indian Ocean and the adjacent land areas, which has turned out to be very important for the future changes in the characteristics of the Indian summer monsoon.

Although the good quality of the simulation by EC-HAM at the high horizontal resolution makes the predicted future changes in the Indian summer monsoon very plausible, one basic source of uncertainty of such predictions remains, namely the choice of the particular scenario for the future emissions of greenhouse gases and aerosols. One can choose from a variety of such scenarios based on different assumptions on the demographic and economic development and on the technical progress (Nakićenović et al. 2000). In the scenario used here (IS92a), for instance, changes in the aerosols have not been considered. Such changes may, however, have an impact on the predicted future changes of rainfall in Southeast Asia, and, hence, affect the future changes in the Indian summer monsoon. According to the review in Cubasch et al. (2001), the effect of sulfate aerosols on the Indian summer monsoon is to dampen the strength of the monsoon compared to that seen with greenhouse gases only. The pattern of response to the combined forcing depends at least partly on the land-sea distribution of the aerosol forcing, which in turn may depend on the relative importance of the direct and indirect effects of the aerosols (e.g. Meehl et al. 1996;

Roeckner et al. 1999). But since for many of the recent SRES scenarios sulphate aerosols peak in the mid-twentyfirst century over South Asia and then decrease to the end of the twentyfirst century (e.g. Cubasch et al. 2001), for the period 2060–2089 the IS92a scenario without any changes in the aerosols is not too far from the recent SRES scenarios, in particular the B2 scenario.

References

Bacher A, Oberhuber JM, Roeckner E (1998) ENSO dynamics and seasonal cycle in the tropical Pacific as simulated by the EC-HAM4/OPYC coupled general circulation model. Clim Dyn 14: 431–450

Bengtsson L, Botzet M, Esch M (1995) Hurricane-type vortices in a general circulation model. Tellus 47A: 175–196

Bhaskaran B, Mitchell JFB, Lavery JR, Lal M (1995) Climatic response of the Indian subcontinent to doubled CO_2 concentration. Int J Climatol 15: 873–893

Chandrasekar A, Kitoh A (1998) Impact of localized sea surface temperature anomalies over the equatorial Indian Ocean on the Indian summer monsoon. J Meteorol Soc Japan 76: 841–853

Cubasch U, Meehl G, Boer GJ, Stouffer RJ, Dix M, Noda A, Senior CA, Raper S, Yap KS (2001) Projections of future climate change. In: Houghton JT, Ding Y, Griggs DJ, Noguer M, van der Linden PJ, Dai X, Maskell K, Johnson CA (eds) Climate change 2001. The scientific basis. Cambridge University Press, Cambridge, UK, pp 525–582

Dickson RR (1984) Eurasian snow cover versus Indian monsoon rainfall – an extension of the Hahn-Shukla results. J Clim Appl Meteorol 23: 171–173

Douville H, Royer J-F (1996) Sensitivity of the Asian summer monsoon to an anomalous Eurasian snow cover within the Météo-France GCM. Clim Dyn 12: 449–466

Douville H, Royer J-F, Polcher J, Cox P, Gedney N, Stephenson DB, Valdes PJ (2000) Impact of doubling CO_2 on the Asian summer monsoon: robust versus model-dependent responses. J Meteorol Soc Japan 78: 421–439

Douville H, Chauvin F, Planton S, Royer J-F, Salas-Mélia D, Tyteca S (2002) Sensitivity of the hydrological cycle to increasing amounts of greenhouse gases and aerosols. Clim Dyn 20: 45–68

Dümenil L, Bauer H-S (1998) The tropical easterly jet in a hierarchy of GCMs and in reanalyses. MPI-Report 247: pp 45

Dümenil Gates L, Hagemann S, Golz C (2000) Observed historical discharge data from major rivers for climate model validation. MPI-Report 307: pp 95

Ferranti L, Molteni F (1999) Ensemble simulations of Eurasian snow-depth anomalies and their influence on the summer Asian monsoon. Q J R Meteorol Soc 125: 2597–2610

Gibson JK, Kållberg P, Uppala S, Hernandez A, Nomura A, Serrano E (1997) ERA description. ECWMF Re-analysis Project Report Series 1: pp 72

Goswami BN, Krishnamurthy V, Annamalai H (1999) A broad-scale circulation index for the interannual variability of the Indian summer monsoon. Q J R Meteorol Soc 125: 611–633

Hagemann S, Dümenil L (1997) A parametrization of the lateral waterflow for the global scale. Clim Dyn 14: 17–31

Hagemann S, Dümenil L (1999) Application of a global discharge model to atmospheric model simulations in the BALTEX region. Nordic Hydrol 30: 209–230

Hagemann S, Dümenil Gates L (2002) Validation of the hydrological cycle of ECMWF and NCEP reanalyses using the MPI hydrological discharge model. J Geophys Res 106: 1503–1510

Hahn DJ, Shukla J (1976) An apparent relation between Eurasian snow cover and Indian monsoon rainfall. J Atmos Sci 33: 2461–2462

Houghton JT, Callandar BA, Varney SK (eds) (1992) Climate Change 1992: the supplementary report to the IPCC scientific assessment. Cambridge University Press, Cambridge, UK, pp 198

Houghton JT, Ding Y, Griggs DJ, Noguer M, van der Linden PJ, Dai X, Maskell K, Johnson CA (eds) (2001) Climate change 2001. The scientific basis. Cambridge University Press, Cambridge, UK, pp 881

Hu Z-Z, Latif M, Roeckner E, Bengtsson L (2000) Intensified Asian summer monsoon and its variability in a coupled model forced by increasing greenhouse gas concentrations. Geophys Res Lett 27: 2681–2684

Huffman GJ, Adler RF, Arkin P, Chang A, Ferraro R, Gruber A, Janowiak J, McNab A, Rudolf B, Schneider U (1997) The Global Precipitation Climatology Project (GPCP) combined precipitation data set. Bull Am Meteorol Soc 78: 5–20

Joseph PV, Eischeid JK, Pyle RJ (1994) Interannual variability of the onset of the Indian summer monsoon and its association with atmospheric features, El Niño, and sea surface temperature anomalies. J Clim 7: 81–105

Ju J, Slingo J (1995) The Asian summer monsoon and ENSO. Q J R Meteorol Soc 121: 1133–1168

Kitoh A, Yukimoto S, Noda A, Montoi T (1997) Simulated changes in the Asian summer monsoon at times of increased atmospheric CO_2. J Meteorol Soc Japan 75: 1019–1031

Krishnamurti TN, Ramanathan Y (1982) Sensitivity of the monsoon onset to differential heating. J Atmos Sci 39: 1290–1306

Lal M, Meehl GA, Arblaster JM (2000) Simulation of Indian summer monsoon rainfall and its intraseasonal variability. Reg Environ Change 1:163–179

Lau N-C, Nath MJ (2000) Impact of ENSO on the Asian-Australian monsoons as simulated in GCM experiments. J Clim 13: 4287–4309

Martin GM (1999) The simulation of the Asian summer monsoon, and its sensitivity to horizontal resolution, in the UK Meteorological Office Unified Model. Q J R Meteorol Soc 125:1499–1525

May W (1999) A time-slice experiment with the ECHAM4 A-GCM at high resolution: The experimental design and the assessment of climate change as compared to a greenhouse gas experiment with ECHAM4/OPYC at low resolution. DMI Scientific Report 99-2: pp 93

May W (2001) The impact of horizontal resolution on the simulation of seasonal climate in the Atlantic/European area for present and future times. Clim Res 16: 203–223

May W (2002) Simulated changes of the Indian summer monsoon under enhanced greenhouse gas conditions in a global time-slice experiment. Geophys Res Lett 29: 10.1029/2001GL013808

May W (2003) The Indian summer monsoon and its sensitivity to the means SSTs: Simulations with the ECHAM4 AGCM at T106 horizontal resolution. J Meteorol Soc Japan 81: 57–83

May W, Roeckner E (2001) A time-slice experiment with the ECHAM4 AGCM at high resolution: the impact of horizontal resolution on annual mean climate change. Clim Dyn 17: 407–420

Meehl GA, Arblaster JM (2002) Indian monsoon GCM sensitivity experiments testing Tropospheric Biannual Oscillation transition conditions. J Clim 15: 923–944

Meehl GA, Arblaster JM (2003) Mechanisms for projected future changes in South Asian monsoon precipitation. Clim Dyn 21: 659–675

Meehl GA, Washington WM (1993) South Asian summer monsoon variability in a model with a doubled atmospheric carbon dioxide concentration. Science 260: 1101–1104

Meehl GA, Washington WM, Erickson III DJ, Briegleb BP, Jaumann PJ (1996) Climate change from increased CO_2 and the direct and indirect effects of sulphate aerosols. Geophys Res Lett 23: 3755–3758

Nakićenović N, and co-authors (2000) Emission scenarios, a special report of Working Group III of the Intergovernmental Panel on Climate Change. Cambridge University Press, Cambridge, UK, pp 599

Rasmusson EM, Carpenter TH (1983) The relationship between eastern tropical Pacific sea surface temperatures and rainfall over India and Sri Lanka. Mon Weather Rev 111: 517–528

Roeckner E, Arpe K, Bengtsson L, Christoph M, Claussen M, Dümenil L, Esch M, Giorgetta M, Schlese U, Schulzweida U (1996a) The atmospheric general circulation model ECHAM-4: Model description and simulation of present-day climate. MPI-Report 218: pp 90

Roeckner E, Oberhuber JM, Bacher A, Christoph M, Kirchner I (1996b) ENSO variability and atmospheric response in a global coupled atmosphere-ocean GCM. Clim Dyn 11: 737–754

Roeckner E, Bengtsson L, Feichter J, Lelieveld J, Rodhe H (1999) Transient climate change simulations with a coupled atmosphere-ocean GCM including the tropospheric sulfur cycle. J Clim 12: 3004–3032

Rupa Kumar K, Pant GB, Parthasarathy B, Sontakke NA (1992) Spatial and subseasonal patterns of the long-term trends of Indian summer monsoon rainfall. Int J Climatol 12: 257–268

Sankar-Rao M, Lau MK, Yang S (1996) On the relationship between Eurasian snow cover and the Asian summer monsoon. Int J Climatol 16: 605–616

Shea DJ, Sontakke NA (1995) The annual cycle of precipitation over the Indian subcontinent: daily, monthly and seasonal statistics. NCAR Technical Note 401 + STR: pp 168

Sontakke NA, Plant GB, Singh N (1993) Construction of all India rainfall series for the period 1844–1991. J Clim 6: 1807–1811

Stendel M, Roeckner E (1998) Impacts of horizontal resolution on simulated climate statistics in ECHAM4. MPI-Report 253: pp 57

Stephenson DB, Chauvin F, Royer J-F (1998) Simulation of the Asian summer monsoon and its dependence on model horizontal resolution. J Meteorol Soc Japan 76: 237–265

Stephenson DB, Douville H, Rupa Kumar K (2001) Searching for a fingerprint of global warming in the Asian summer monsoon. Mausam 52: 213–220

Stratton RA (1999) A high resolution AMIP integration using the Hadley Centre model HadAM2b. Clim Dyn 15: 9–28

Timmermann A, Oberhuber J, Bacher A, Esch M, Latif M, Roeckner E (1999) Increased El Niño frequency in a climate model forced by future greenhouse warming. Nature 398: 694–697

Voss R, May W, Roeckner E (2002) Enhanced resolution modelling study on anthropogenic climate change: changes in extremes of the hydrological cycle. Int J Climatol 22: 755–777

Webster P (1983) The large-scale structure of the tropical atmosphere. In: Hoskins B, Pierce R (eds) Large scale dynamical processes, Academic Press, San Diego, pp 235–276

Webster PJ, Yang S (1992) Monsoon and ENSO: selectively interactive systems. Q J R Meteorol Soc 118: 877–926